Universiteit Utrecht

Impact of in-situ ageing on the mineralogy and mechanical properties of Portland-based cement in geothermal applications

Anastasia Papaioannou

Thesis for the degree of Master of Science

Department of Earth Sciences Utrecht University

1 st supervisor: prof. dr. Chris Spiers

2 nd supervisor: prof. dr Hans de Bresser

January 2018

Contents

Abstract 3
1. Introduction 4
1.1 Geothermal energy and geothermal systems 4
1.2 Research question 5
1.3 Research aim 5
2. Geothermal Well Design 7
2.1 Wellbore construction 7
2.2 The role of the cement sheath 8
3. Composition and properties of wellbore cement 9
3.1 Conventional, oilwell and geothermal wellbore cements 9
3.2 Downhole behaviour and physical properties of class G Portland cement 11
3.2.1 Shrinkage 11
3.2.2 Porosity 11
3.2.3 Degradation of cement composition and strength 12
4. Geomechanics of wellbores 16
4.1 Direct effects of pressure and stress changes 17
4.2 Direct effects of thermal stresses 18
4.3 Effects of thermal pressurization of pore fluid and associated poroelastic response 19
5. Present Experiments 20
5.1 Materials and sample preparation 20
5.2 Experimental and analytical methods 21
5.3 Results 23
5.3.1 Mineralogy – XRD data 23
5.3.2 Microstructure 25
5.3.4 Mechanical data and strength 28
6. Discussion 31
6.1 Present experiments 31
6.2 Comparison with related studies 33
6.3 Future Work 36
7. Conclusions 38
Acknowledgments 40
Appendix 1 41
Appendix 2 42
References 43

Abstract

This study aims to review the current knowledge on wellbore cement degradation under high pressure and temperature conditions and to experimentally investigate whether the standard methodology used for cement durability assessment can adequately describe the performance of a cement formulation at low and high temperatures. During operation the wellbore undergoes many cycles of cooling down and warming up, a process that exposes the comprising parts of the wellbore to heavy loads due to thermal stresses and strains. These thermal effects can compromise the wellbore's operational integrity by damaging the steel casing, cracking the cement or by disrupting the bond at the interfaces cement-casing or cement-formation. Such cases of annular cement failure occur frequently in geothermal wellbores that encounter high pressures and temperatures. The special cement formulation containing 40% quartz flour, that is designed for use in wellbores operating at temperatures higher than 110 °C and is recommended by the Oil and Gas industry was used in the experimental part of this study. Two series of samples were examined. The first series was exposed to 60 °C, while in confinement, and the second was exposed to hydrothermal conditions of 120 °C and 2 bars for a total of 42 days. The selected exposure temperature of 60°C corresponds to the average wellbore temperature the cement experiences after placement in-situ, for the one month, before the wellbore becomes operational again. On the other hand, the exposure temperature of 120 °C was selected in order to determine the performance of this cement formulation just above the crucial temperature of 110 °C where cement strength retrogression occurs. Mineralogy and microstructural features of the samples were examined through XRD, SEM and optical microscopy after 28 days of exposure to accurately depict the period of cement sheath in-situ ageing. Maximum compressive strength and Young's modulus values were obtained through uniaxial compressive tests at 2, 3, 7, 14, 28 and 42 days of exposure. The results showed that the quartz flour contained in this formulation does not react at all when exposed to 60 °C for 28 days while only 50% of it react when exposed to 120 °C for the same time. The compressive strength and Young's modulus is higher when exposed to the hydrothermal conditions, while the porosity is lower due to precipitation of hydrates in the pores at higher temperatures. Finally, the present experiments indicate that exposure to higher temperatures increases the stiffness of the hardened cement paste of this formulation. High stiffness of the sealant indicates a slower and more brittle mechanical response of the cement sheath to the expansion and contraction of the steel casing, and increases the probability of cement sheath shear failure. Further comparison of this formulation with the standard cement used in the geothermal wellbores would require determination of its porosity ad permeability. Complete evaluation of its performance under HPHT conditions requires determining its coefficients of thermal expansion, its thermal and elastic properties, its tensile and compressive strengths and its initial state of effective stress. This could be achieved by performing triaxial tests and by using the methodology applied by rocks mechanics to determine the performance of porous materials.

1. Introduction

The increasing worldwide interest in energy production from sustainable sources is driven not only by the awareness of the effects of fossil fuel combustion on the environment, but also by the realization that the fossil fuel deposits are only a few decades away from depletion. Although the majority of the energy produced, still comes from fossil fuels and nuclear energy, 81,7% in 2014 (IRENA, 2017), the contribution of renewable energy sources is expected to increase to 30-80% by 2100. Currently, the electricity generated by renewable energy sources is produced, in order of decreasing contribution, by hydropower, biomass, geothermal, wind and solar energy (Fridleifsson, 2001). Geothermal energy has a potentially large contribution to make in volcanic regions, such as in the case of Iceland where approximately 26% of the country's electricity is produced by five major geothermal power plants (Saemindsson, Axelsson and Steungrimsson, 2009) but also a major contribution to heat energy supply more generally, including the ground source heat pumps (GSHP) widely used in the Netherlands, that serve as a building's central heating/cooling system by transporting heat to and from the ground. (Hanova, 2007). One of the barriers to introducing geothermal energy is the issue of wellbore integrity at high T in-situ conditions not normally experienced in conventional well design. This thesis deals with the topic of well cement behaviour in this context.

1.1 Geothermal energy and geothermal systems

The term "Geothermal energy" is used nowadays to refer to that part of Earth's thermal energy that can be recovered and exploited by man. The heat contained in the Earth's interior moves in the form of thermal energy outwards from the hot Earth's core towards the mantle and crust. This heat flow results in temperature increasing per unit distance of depth, forming a temperature gradient with increasing depth, the geothermal gradient. Different tectonic environments generate different geothermal gradients, with the average geothermal gradient being 30°C/km. As a result, potential sources of geothermal energy can exist in many regions, forming different types of geothermal systems.

In general, a geothermal system is composed of three elements: a heat source, a reservoir and a fluid which acts as the heat transport medium. Although a standard classification method does not exist, most of the largest geothermal fields around the world are characterized as either high - or low - temperature geothermal fields. High temperature geothermal systems have been utilized for electricity production for more than a hundred years. Most of these geothermal systems operate at temperatures of 150-300°C, while higher temperature geothermal systems operate at temperatures higher than 250 ° C. The later are almost always located near areas with elevated geothermal gradient such as active volcanic centers, rift zones, hot spots. The thermal energy potential of the magmatic systems is thought to be much higher than the hydrothermal systems, but it is probably because of

the technical issues related to drilling deep and in such high temperatures that very few wells were able to actually approach the roots of the hydrothermal systems and withstand conditions close to the critical point of water (T > 374°C, P > 221 bar) (Dobson *et al.*, 2017). Moreover, the interest in exploitation of supercritical fluids was encouraged by recent studies showing that these fluids have high rates of mass transport and much higher productivities, giving a much higher economical potential to wells tapping supercritical fluids. This knowledge is the reason many new studies are focusing on, not just identifying challenges, but also attempting to optimize approaches, techniques and materials related to drilling in high pressure – high temperature (HPHT) or supercritical conditions.

1.2 Research question

The success of such geothermal operations is directly linked to sustaining the wellbore integrity during the stress changes induced by downhole variations of pressure and temperature. Wellbore integrity is defined in this study as the control and maintenance of flow inside the wellbore and is secured by maintaining the good bonding of the cement sheath with the steel casing and the surrounding formation. Although there are many studies on the cement mineralogy, microstructure and durability at high temperatures, their results cannot be used when studying cement performance at in-situ HPHT geothermal conditions. This is because they either address cement exposure in high temperature under atmospheric pressure, or they are performed on the standard Portland cement used for wellbore construction and not on the cement formulation for geothermal applications, or they just have been performed at outdated “high temperatures” that have long been exceeded in terms of geothermal energy production ambitions. As a result, current knowledge of cement mineralogy, microstructure and especially mechanical behavior under HPHT or supercritical geothermal conditions is insufficient for current aims, operational performance needs and integrity or safety needs.

1.3 Research aim

In the life of a well, numerous factors play an important role in maintaining wellbore integrity. In a drilling stage, it depends mainly on proper selection of wellbore components such as drilling mud, steel casing and cement slurry but also proper monitoring of the wellbore’s pressure for gas intrusion, adequate removal of drilling mud before cementing and proper placement of the steel casing.(Shadravan *et al.*, 2015a). During the production phase, wellbore integrity strongly depends on maintaining the bonding between formation, cement sheath and steel casing.

In HPHT wells, during the production process, the pressure differential inside the casing and the surrounding formation is larger than the conventional wells. The stress induced by fluid withdrawal in highly compact reservoirs can cause the cement and the casing failure in these wells. These present a greater challenge to wellbore integrity than in conventional wells. The present work aims to improve understanding of the mechanisms that drive cement degradation in geothermal and deep oil well

conditions. The first part of this study (Chapter 2 to 4) focuses on a review of what is known on the impact of HPHT ageing conditions on cement mineralogy and mechanical behavior, as well as the mechanical challenges the cement sheath and wellbore integrity face during HPHT geothermal operation. In the second part (Chapter 5), the mineralogical, microstructural and mechanical properties of the commercially available cement formulation for geothermal wellbores are determined experimentally. Uniaxial compressive tests, XRD and SEM analyses are performed, serving as a first step to confirm the lower temperature properties of the cement for geothermal applications. The tests are performed in samples of the special cement formulation that were aged under confined conditions at 60 ° C and under hydrothermal conditions at 120 ° C. By performing the standard tests used by the cement industry, we assess the suitability of the methods to reliably evaluate the performance of this cement formulation at low and high temperatures. In this way, this study aims to serve as a basis for future work on cement formulations for HPHT conditions and on experimental methods used to properly assess their performance at HPHT conditions.

2. Geothermal Well Design

2.1 Wellbore construction

Geothermal wellbore construction follows the same principles as the telescopic wellbore construction for oil and gas exploitation (Teodoriu and Falcone, 2008). It involves drilling a borehole and inserting a casing which is sealed and stabilized with the use of a Portland-based cement. While the wellbore is drilled, drilling mud is pumped down through the bore of the drill pipe and up between the walls of the drill column and the wall rock as illustrated in Fig. 1. The drilling mud circulation cools down and lubricates the drill bit, prevents inflow of formation fluids and carries rock cuttings back to the surface (Lavrov and Torsæter, 2016c).

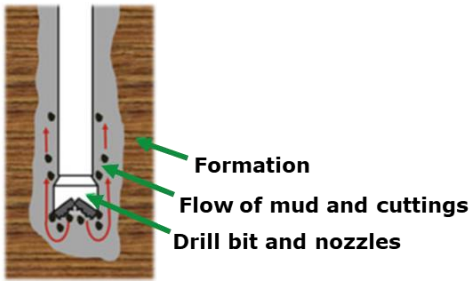

Figure 2. Schematic illustration of drilling process (after Lavrov and Torsæter, 2016)

When the desired depth is reached, the drill pipe is retracted and a string of steel casing tubes is put together and run down to the bottom of the hole with the drilling mud still in place. Subsequently, the drilling mud must be removed and replaced by cement slurry. In order to remove the drilling mud, fluids, called washer and spacer fluids, are pumped down the casing bore and up between the outer casing surface and wall rock to the surface. In the same manner, cement slurry is pumped down the bore and is forced upward as seen in Figure 2, filling this way the annular space between the casing and the wall rocks, forming what is termed the cement sheath.

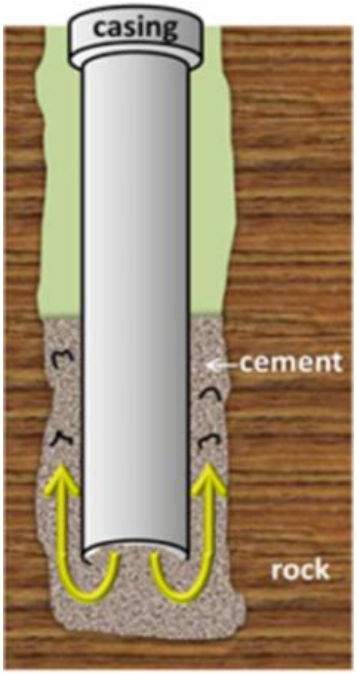

Figure 1. Schematic illustration of cementing operation (after Lavrov and Torsæter, 2016)

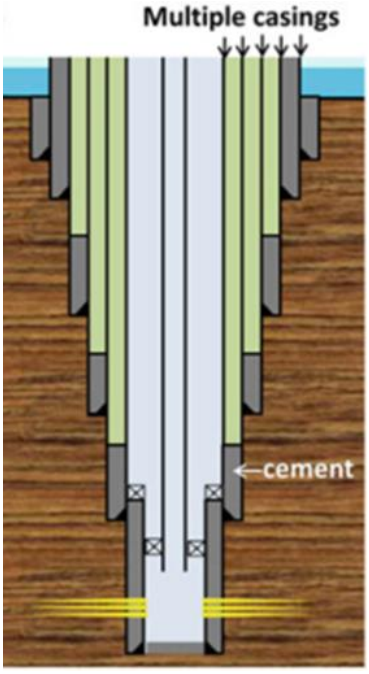

Since the casing installed is smaller in diameter than the drill bit used, progressively smaller diameter bits and casing strings are used to drill the wellbore (Nelson and Guillot, 2006). This results in the telescopic profile illustrated in Fig. 3, characteristic for the deep wellbores used in the oil and gas and geothermal operations.

Figure 3. Schematic illustration of final telescopic structure of a finished well (after Lavrov and Torsaeter, 2016)

2.2 The role of the cement sheath

The main function of cement sheath in wellbores is to secure in place and support the weight of casing inside the well and to provide zonal isolation, i.e. to prevent exchange of fluids between the different units in the sedimentary sequence penetrated by the well, i.e. by blocking communication of formation fluids at different levels.

Disrupted zonal isolation could occur as a result of problems appearing either at the pre-production or during the production phase. They have been named and classified respectively by Teodoriu *et al.*, 2013 and Shadravan *et al.*, 2015b. According to them in the pre- production stage, problems associated with the drilling and cementing process and involve the formation damage during drilling (or caving), casing decentralization due to incomplete cementing, inadequate drilling mud removal, incomplete cement placement,) cement shrinkage, inadequate formation-cement/cement-casing bond, and contamination of cement by mud or formation fluids. In the production phase, zonal isolation can be compromised by mechanical stresses that are induced in the cement sheath by pressure and temperature changes during the production cycle. On the other hand, the mechanical stresses can cause the formation of micro-fracturing at the cement-casing interface or the disruption of the bonding between cement and formation that are further described in section 4.1.

Overall, from the above it can be seen that the vast majority of problems that can disrupt the wellbore's zonal isolation are related to cement. Thus, a properly constructed cement sheath is essential for the well integrity. Well integrity, in the present study, refers to the control and maintenance of flow inside the wellbore.

3. Composition and properties of wellbore cement

3.1 Conventional, oilwell and geothermal wellbore cements

Oilwell cement is not the same as concrete used in the construction industry. Dry cement is produced by first pulverizing raw materials (mainly calcium oxide, silica, alumina and iron compounds). The powder is then converted to a clinker by heat treatment in a rotary kiln (typically at 1450 °C), and the finished cement powder is produced by grinding the clinker with gypsum. The latter controls the solidification time and how quickly the cement builds up strength during hardening. The clinker consists of 50–70 % alite (Ca_3SiO_5 or C_3S), 15–30 % belite (Ca_2SiO_4 or C_2S), 5–10 % aluminate ($Ca_3Al_2O_6$ or CA) and 5–15 % ferrite (Ca_2AlFeO_5or CAF), plus small amounts of other phases (Nelson and Guillot, 2006). The dry cement powder reacts quickly and strongly with water, and solidifies and develops compressive strength as a result of hydration. This is a process involving complex reactions between water and the cement oxides.

A cement slurry is a mixture of cement and water in such proportion that solidification can occur. The water-to-cement ratio refers to proportions by mass, and they are typically in the range of 0.3–0.6 for well cement. The solidification starts with setting, which is a rapid stiffening without significant strength development, followed by the slower hardening process which builds compressive strength. The main constituents of hardened cement paste are calcium hydroxide (CH or Portlandite) and a nearly amorphous calcium silicate hydrate, C–S–H. They formed during hydration of the main and secondary clinker phase, alite (C_3S) and belite (C_2S) respectively. The hydration products of belite (C_2S), are also CH and C–S–H but there is a lower relative amount of CH compared to the one resulting from C_3S hydration. C_2S is much less soluble than C_3S, so the rate of hydration is much slower. Even though C_2S hydration contributes little to the early strength of cement, it makes substantial contributions to the strength of mature cement paste and concrete (Taylor, 1990). Research has so far not managed to come up with one well cement formulation that alone could overcome all the problems associated with primary cementing. Cement slurries are thus optimized with regard to only a few challenges at a time.

Almost all the standard wellbores use Portland based cements that can be formulated differently in order to achieve the best cement performance in the wellbore conditions. The American Petroleum Institute has developed a system for oil well classification and performance, the 10A API specification, according to which most oil well cements are manufactured and selected for use. This system recognizes 8 classes of Portland cement classified based on chemical, physical and performance requirements. The API classifications can be found in the Appendix 1 Tables A1 a and b.

Table 1 .Average composition of ordinary Portland cement clinker and typical composition of Portland cement type G

Composition	Ordinary Portland cement (Nelson and Guillot, 2006)	Cement type G (PetroWiki)
alite (Ca_3SiO_5 or C_3S),	50–70 %	58%
belite (Ca_2SiO_4 or C_2S)	15–30 %	19%
aluminate ($Ca_3Al_2O_6$ or C_3A)	5–10 %	2%
ferrite ($Ca_4Al_2Fe_2O_{10}$or C_4AF)	5–15 %	11%

Oilwell cements are manufactured using the normal raw materials and processes employed as for ordinary, moderate or high sulphate resistant Portland cement. This means, that the compound composition obtained after production as well as after hydration will, of course, vary but within the set limits of the appropriate specification. Control over the compound compositions allows for control over the slurry performance. The key factors in determining which class a basic oilwell cement belongs to are the performance tests.

Table 2 Typical mill run analysis of Portland cement type G (PetroWiki)

Oxide	Class G, wt%
Silicon dioxide, SiO_2	21.7
Calcium oxide, CaO	62.9
Aluminum oxide, Al_2O_3	3.2
Iron oxide, Fe_2O_3	3.7
Magnesium oxide, MgO	4.3
Sulfur trioxide, SO_3	2.2
Sodium oxide, Na_2O	
Potassium oxide, K_2O	
Total alkali as Na_2O	0.54
Loss on ignition	0.74
Insoluble residue	0.14
Phase Composition	
C_3S	58
C_2S	19
C_3A	2
C_4AF	11
Physical Properties	
% passing 325 mesh	87
Blaine fineness, cm^2/gm	3,470
Physical Requirements	
Thickening time, min, Sch 5	1:40
B_c at 30 min	14
8 hr compressive strength, 110°F (38°C)	928 psi (6.4 MPa)
8 hr compressive strength, 140°F (60°C)	2,247 psi (15.5 MPa)
Free fluid, mL[13]	4.4

The most common cement used in geothermal well construction is type G. This is because oil well Portland cement type G exhibits low viscosity, fluid loss control, predictable thickening time and the tendency not to segregate while it shows constancy in high sulfate resistance, high durability and mechanical strength (Nelson and Guillot, 2006). A typical chemical analysis of type G cement can be found in Table 2.

3.2 Downhole behaviour and physical properties of class G Portland cement

3.2.1 Shrinkage

Cement powder is mixed with water at the rig site, and the slurry is pumped down the casing. After reaching bottomhole, the cement enters the annulus behind the casing, and pumping continues until an annular cement sheath of a required height is created. Cement is then left in the annulus to harden. The hardening is due to hydration of cement which starts immediately or sometime after the cement slurry has been mixed. Hydration involves changes to both the structure and the properties of cement. In particular, the density of hydration products is higher than that of the original unhydrated phases (Nelson and Guillot, 2006. When there is not an extra water supply, neat cement to shrinks. There have been reported shrinkage-induced reduction examples of cement bulk volume in the range of 0.5–5 % (Nelson and Guillot, 2006). Due to chemical shrinkage, i.e. shrinkage due to hydration reactions, porosity and pore pressure decrease as setting proceeds. If an external water supply is available, the decline of pore pressure leads to water being sucked into the cement's pore space. Water availability reduces the bulk shrinkage of cement and may even cause bulk expansion. In addition to the reduction in porosity and pore pressure, shrinkage may even cause fracture growth in cement (Dusseault et al., 2000). It may also lead to the development of a microannulus between the cement and the formation, which is one of the mechanisms resulting in wellbore leakage.

3.2.2 Porosity

Porosity is defined as the ratio of the pore volume to the total (bulk) volume of the material. If a porous material contains a connected pore system, applying a pressure gradient to the pore fluid will put the fluid in the pore space into motion. Flow of a Newtonian fluid through a porous medium, such as a cement slurry undergoing solidification, can be described by Darcy's law. The total discharge Q (m^3/s) can then be calculated as follows:

$$Q = -kA\, dP/m\, dX$$

where X points in the direction of flow; A is the cross-section area normal to flow (m^2); P is the pore pressure (Pa); μ is the dynamic viscosity of the pore fluid (Pa s). The coefficient k (m^2) is the absolute permeability (Lavrov and Torsæter, 2016b).

Cement hydration leads to an inter-granular porosity in the final product because the volume occupied by the reaction products (cement hydration products + water) is less than the volume occupied by the initial reactants (reactive cement powder + water). Intra-granular porosity also exists in the CSH grains, while Portlandite grains can be considered as non porous (Ulm, Constantinides and Heukamp, 2004).

Therefore, the cement is a porous material and as such the mechanical behavior of hardened cement paste can be described within the framework of the theory of poro-mechanics (Ghabezloo *et al.*, 2008)

The permeability of a cement slurry is on the order of 10^{-12} m^2 (1 D), while the permeability of hardened cement is on the order of 10^{-18}–10^{-17} m^2 (1 to 10 µD). Rapid decline of permeability during setting is mentioned as a key quality of good wellbore cement although is not easy to measure the exact slurry permeability (Appleby and Wilson, 1996). Conventional steady-state permeability measurements with water as the flowing fluid show poor reproducibility and significant scatter for cement slurries. On the other hand, using gas as the flowing fluid promotes cement drying, shrinkage and fracturing .(Lavrov and Torsæter, 2016b)

3.2.3 Degradation of cement composition and strength

Temperature

Increasing temperature does not only cause physical changes of cement. The impact of high temperature in cement chemistry is probably the most compromising factor in well integrity. The different phases formed at different temperatures have been compiled in a " phase diagram" by Taylor (1990) – see Figure. 4.

At or near ambient conditions, the Ordinary Portland cement - OPC (used here to refer to class G oilwell cement) hydration produces the amorphous C-S-H and the crystalline $Ca(OH)_2$ resulting in a final product that is a mixture of ordered and disordered phases. C-S-H has been found to be the highly disorder version of the crystalline phases Tobermorite and Jennite (Taylor, 1990). Although XRD analyses suggest a similarity in terms of pattern appearance, with those two crystalline phases, the crystal structure of Jennite is still not known while Tobermorite has a C/S of 0,83 when C-S-H in OPC has a C/S of 1,7 to 2 (Hong and Glasser, 2004). Overall, amorphous C-S-H or "gel" is, at ambient conditions, the main hydration phase of OPC no matter the C/S composition and although thermodynamically unstable at all temperatures it is very persistent as it has even be detected in uncarbonated Roman mortars.

At temperatures above 110°C, the reactions result in different hydration products. Thorvaldson and his co- workers first found that alpha dicalcium silicate hydrate, α-C_2SH [$Ca_2SiO_3(OH)_2$, was formed when ordinary Portland cement (OPC) was cured at this temperature. At high temperatures, dicalcium silicate is present and there is no evidence of a monocalcium silicate. Thus, there is a distinct difference in the hydration products at normal temperatures and at temperatures above 110 ° C. (Patchen, 1960). The lime-rich alpha-dicalcium silicate hydrate (α-C_2SH) is denser than the usual calcium silicate hydrate (C-S-H gel) product and can undergo deleterious bulk volume decrease either via shrinkage or in terms

of porosity, resulting in a decrease in cement strength and increase in permeability. This phenomenon is known in cement chemistry as *strength retrogression* (Patchen, 1960; Pernites and Santra, 2016).

Cement strength retrogression is a serious problem for the wellbore and all types of OPC and oilwell cements show lower strengths when cured above 110 ° C compared to 93 ° C. As OPC has a calcium oxide to silicon dioxide (C/S) ratio close to 3.1 (Figure 2), crystallization of the dicalcium form of silicate hydrate is favored. An established chemical strategy to prevent strength retrogression is addition of silica in order to decrease the C/S ratio and to force the reaction toward the monocalcium forms which possess high strength and low permeability (Patchen, 1960). This is because when temperature increases in the presence of a siliceous additive such as fly ash, silica fume or silica (quartz) flour the $Ca(OH)_2$ is being consumed resulting in a C-S-H of a lower C/S ratio. Patchen (1960) calculated that a dosage of 35 to 40% by weight of cement (bwoc) is enough to prevent the reaction forming α-C_2SH and instead allow the development of silica-rich cement phases like Tobermorite or Xonotlite. Moreover, this formulation, in a water to solids ratio of 0.4, results in 91% of the water being chemically bound against only 39 % of the available water in the average oilwell cement It has since been considered the optimum concentration and when cement is intended for autoclaving, where bulk C/S ratios of 0.8-1.5 are preferred, silica flour is usually added.

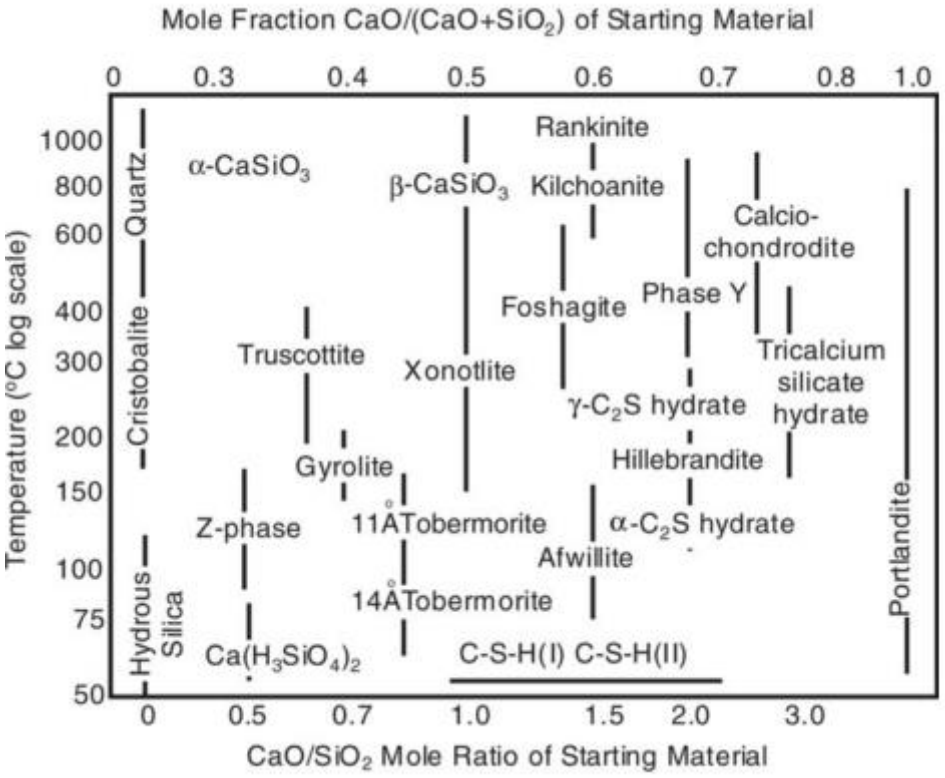

Figure 4. Phase diagram of the $CaO–SiO_2–H_2O$ system from 50 to 1000 °C. The vertical lines indicate the C/S mole ratios of the phases. As emphasized by Taylor, this is not an equilibrium diagram, but "merely represents the conditions under which each phase is most usually obtained". Diagram from (Taylor, 1990)*, with modifications after* (Meller, Hall and Phipps, 2005)

Pressure

There has been a plethora of studies on the impact of temperature on the hydration products of OPC and OPC with silica addition, and it was pointed out early on that the conditions, under which the cement exposure in high temperature took place, are of detrimental importance. As with every aqueous system, phase relations in the $CaO\text{-}SiO_2\text{-}H_2O$ system depend not only on the temperature but also the pressure and the H_2O availability during and after the phases' formation. Exposure to high temperature at atmospheric humidity can cause significant loss of H_2O, as opposed to exposure to high temperature at saturated steam pressures. Conditions described by the presence of aqueous solutions at temperatures high enough to generate saturated steam pressure are also referred to as hydrothermal conditions. In the case of the cement sheath in geothermal operations, cementing takes place at an average temperature of 60 ° C, obtained and maintained by continuous recirculation of fluid in the wellbore. Moreover, the cement sheath is restricted on one side by the steel casing and on the other by the surrounding formation. Considering that the surrounding formations, in geothermal systems where HPHT conditions are encountered, have usually a lower permeability than the cement, we can assume that cement hardening and exposure to high temperature occurs under confinement. As such, the cement phases and microstructure obtained in the cement sheath they would resemble those obtained under hydrothermal rather than ambient conditions.

The difference when hydration when occurs under hydrothermal conditions is that the C-S-H gel converts rapidly to crystalline phases. For instance, cement formulations with quartz flour when autoclaved, form the desired monocalcium minerals like Tobermorite and Xonotlite in high yields of more than 50%, in 12-18 hours at 160-190 ° C. Despite their crystallization in short autoclaving times, when longer duration of autoclaving is applied, the high yields of crystalline phases like Tobermorite decline, implying that they are obtained as a result of rapid crystallization under metastable conditions. In fact Xonotlite forms at higher temperatures than Tobermorite, with the equilibrium phase boundary between the two minerals being at approximately 140°C , (Gabrovšek *et al.*, 1993)

Presence of Al_2O_3 in the $CaO\text{-}SiO_2\text{-}H_2O$ system

When examining the cement phase relations at high temperatures, another consideration should be taken into account. As mentioned in subchapter3.1, there is some aluminium content in the cement clinker, found in the ferrite and aluminate phases which is often omitted from calculations. Although a small amount it is enough to make the OPC not a pure $CaO\text{-}SiO_2\text{-}H_2O$ system but rather a $CaO\text{-}Al_2O_3\text{-}SiO_2\text{-}H_2O$ system. In this system hydrogarnet is the most common aluminum-bearing secondary phase produced. It is a mineral that displays solid solution from grossular (y=0) to katoite (y=3), with the general formula $C_3AS_{3-y}H_{2y}$. Experimental work on this system (Kyritsis *et al.*, 2009) showed that more than one distinct hydrogarnet composition is usually present in this system and it appeared to depend

on the temperature and the C/S ratio of the sample, with y decreasing with decreasing C/S and increasing temperature. In the presence of alumina in the system, not only aluminum bearing phases become dominant, but the stability fields of Al-free phases are pushed in higher temperatures. Tobermorite becomes the more stable phase as the aluminium content is increased and temperature decreased while with increasing temperature and decreasing aluminium content, Xonotlite becomes the more stable phase(Shaw, Clark and Henderson, 2000).

Besides the effect on the phase relations, curing and exposure of cement in hydrothermal conditions causes significant changes in the pore structure of hardened cement pastes. Kuzielová *et al.*, (2017) reported the decrease of large pores (> 50 nm) with simultaneous rise of mesopores (4.5–50 nm) and gel pores (<4.5 nm) on cement formulations with silica (silica fume, SF) and alumina (blast furnace slag, BFS) admixtures when cured under hydrothermal conditions. This pore "refinement" or "consolidated pore structure" was attributed to the higher extend of crystallization at these conditions, causing the transformation of C-S-H to Tobermorite and other C-A-S-H phases, as well as to the formation of carbonates. The carbonates formation is explained in the same study to occur not only from Portlandite carbonation, but also from carbonation of other phases that form at higher replacement levels

It becomes apparent then that although the favorable conditions and compositions for crystallization of each constituent phase are well known, the phase relations in the CaO-Al_2O_3-SiO_2-H_2O system are rather complex as they greatly depend on the pressure and temperature conditions that occur during hydration and exposure.

4. Geomechanics of wellbores

When a wellbore is drilled, the rock that originally occupied the borehole volume, is removed. This results in stress concentration around the hole since the rock that was supporting the formation is not there anymore. During drilling, mud exerts pressure on the borehole wall, which reduces the stress concentration around the hole. However, it is, not possible to exactly restore the original state of stress around the hole by applying wellbore pressure. After setting the steel casing and cementing the annulus, the disturbance to the stress field is still there. If the casing pressure is changed or the casing is heated or cooled, the stress disturbance around the hole may be amplified, possibly leading to cracks developing in casing, cement or rock in the near-well area. Similarly, the near-well stresses may be affected by in situ stress changes in the reservoir caused by depletion or by injection of fluids (Philippacopoulos and Berndt, 2002; Lavrov and Torsæter, 2016a)

In a circular wellbore with a centered casing, the principal stresses are the radial stress, the hoop stress (also known as the circumferential stress), and the axial stress (Lavrov and Torsæter, 2016a). The axial stress is directed along the wellbore axis and the directions of the other two principal stresses are as illustrated in Figure 5.

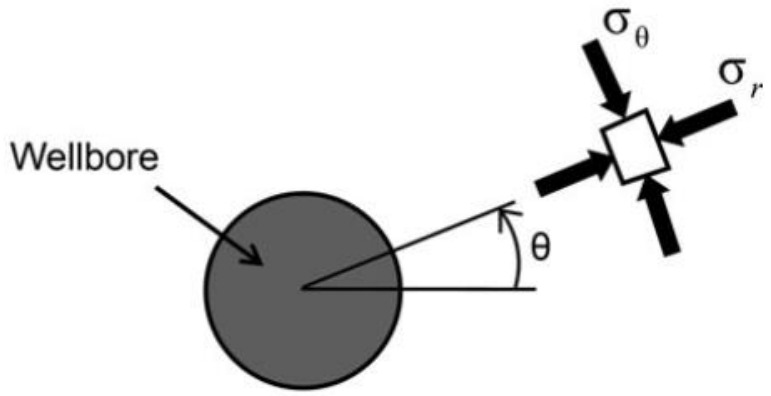

Figure 5 Orientation of radial stress σ_r, and hoop stress, σ_h, in the vicinity of the well (Lavrov and Torsæter, 2016)

Changes in the fluid pressure and/or temperature related to the wellbore operation can cause cement failure. The type of failure that may occur, is controlled by the absolute and relative magnitudes of the principal stresses in cement. Three main types of mechanical failure of annular cement are possible (Teodoriu *et al.*, 2013; Lavrov and Torsæter, 2016a)

• debonding at the casing-cement interface and or at the cement-rock interface;

• radial fractures in cement;

• shear failure of cement;

4.1 Direct effects of pressure and stress changes

Radial cracks form in cement when the effective hoop stress exceeds the tensile strength of cement (Figure 6a). Debonding (Figure 6b). occurs at the casing-cement interface when the effective radial stress at the interface exceeds the tensile strength of the interface Respectively, debonding at the cement-rock interface occurs when the effective radial stress at the interface exceeds the tensile strength of the interface. Both types of debonding will eventually result in the development of a microannulus along the wellbore that may compromise zonal isolation. Finally, shear failure of cement (Figure 6c)may occur when all the principal effective stresses are compressive and such that the shear strength of cement is exceeded (Teodoriu *et al.*, 2013; Lavrov and Torsæter, 2016a)

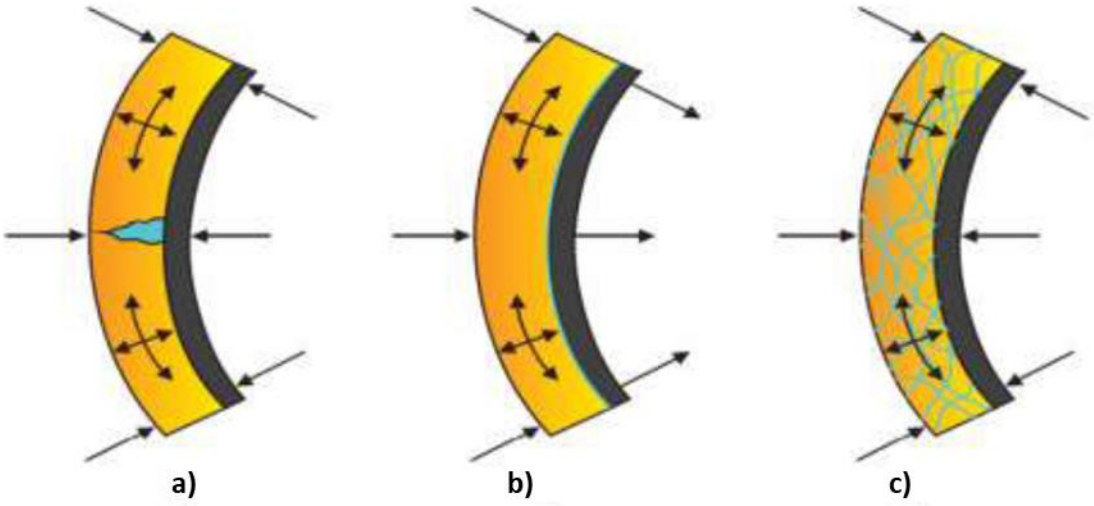

Figure 6. Schematic illustration of a) formation of radial cracks in cement sheath, b) debonding at cement-casing or cement-rock interface and c) shear failure of cement (after Teodoriu et al.*, 2013)*

4.2 Direct effects of thermal stresses

Expansion and contraction of the casing can be caused not only by casing pressure variations, but also by in – situ temperature changes in the well. This is especially important for HPHT wells. When the temperature of the casing changes, the casing expands (increasing temperature) or contracts (decreasing temperature). Inevitably, these mechanical deformations affect the cement sheath. Furthermore, as the temperature change propagates into the cement and the rock, these materials might expand or contract, too(Lavrov and Torsæter, 2016a). The thermal stresses produced as a result of such contraction or expansion will be determined by the relationship between coefficients of thermal expansion and elastic properties of casing, cement and rock. Consequently, the eventual effect of thermal stresses depends on the initial state of stresses in cement. If significant compressive initial stresses are induced in the cement sheath during hardening such as in the case of an expansive cement, the predominant mode of failure during subsequent thermal loading may be compressive (shear). If the initial stresses are not very high or are zero, as in the case of a shrinking cement, tensile cracks and debonding may occur.(Thiercelin *et al.*, 1997).

It is clear then that initial state of stress is a crucial parameter when someone evaluates the stresses a material can withstand before failure as it sets the initial distance from failure (Ghabezloo *et al.*, 2008). The initial state of stress of a material can be described as the state of stress that exists within the material prior to any additional loading. For porous media characterization of initial stress is more difficult because it also requires accounting for pore pressure and it corresponds to Terzaghi effective stress (Terzaghi 1943):

$$\sigma_{eff} = \sigma - P_f$$

σ_{eff}:·effective·stress,·P_f·:·pore·fluid·pressure,·σ:·total·stress

4.3 Effects of thermal pressurization of pore fluid and associated poroelastic response

The increase of temperature in porous materials in the presence of water can generate volume change due to increase in pore fluid pressure. This pressurization of the pore fluid results from the difference between the thermal expansion coefficients of the solid phase and the pore fluid. (Ghabezloo, Sulem and Saint-Marc, 2009). This is important in simulating in-situ conditions where wellbores undergo sudden temperature changes although studies on wellbore cement tend to neglect the poromechanical effects when examining the cement sheath mechanical properties (Lavrov and Torsæter, 2016a). An increase of the pore fluid pressure causes a reduction of the effective mean stress, that could eventually result in shear failure or hydraulic fracturing. This is for example the case at steam injection geothermal operations where the rapid increase of temperature could cause damages to the wellbore's cement sheath leading to loss of zonal isolation.

Studies on the effect of undrained heating and the phenomenon of thermal pressurization on a fluid saturated cement paste have been performed by Ghabezloo, Sulem and Saint-Marc (2009). In this study the drained thermal expansion coefficient (pore pressure increase due to a unit temperature increase of the hardened cement paste was measured in a drained heating test and found equal to $6\times10^{-5}(°C)^{-1}$. The undrained heating test that was combined with a heating-cooling cycle showed that the pore fluid pressure changes proportional with temperature change. This proportional change was described in the form of a constant thermal pressurization coefficient that is equal to 0.6 MPa/°C. Nevertheless, this coefficient is anticipated to vary during the heating and cooling phases as thermal expansion of water also varies with temperature.

5. Present Experiments

5.1 Materials and sample preparation

For the experiments conducted in this study, 74 specimens were prepared using Dyckerhoff HT Basic Blend of cement clinker (API class G cement with 40 % silica flour). The oxides analysis of the cement is summarized in Table 3 while Table 4 is an overview of the experiments and analyses performed. The cement slurry was prepared according to the company's specifications, using de-ionized water in a water to solid (cement + silica flour) ratio of 0.371. For the mixing process, the EN 196-3 protocol was followed. Upon preparation, the slurry was poured into PVC cylindrical moulds with 25 mm internal diameter and 60 mm length. Pouring into the cylindrical moulds was facilitated by the use of a syringe in order to achieve homogeneity and minimize air entrapment. Standard prisms of 40 mm x 40 mm x 160 mm were casted in stainless steel moulds. The cement slurry was prepared in small batches in order to minimize casting time and avoid segregation and water separation. Upon casting, the moulds were sealed on top by caps that were glued on them to ensure confinement.

Table 3. Oxides analysis of Dyckerhoff HT Basic Blend by x-ray fluoresence .

Oxides	SiO_2	Al_2O_3	CaO	MgO	$Fe2O_3$	Na_2O	K_2O	Mn_3O_4	TiO_2	P_2O_5	SrO	NiO	V_2O_5	BaO	ZrO_2
Weight %	44.3	2.9	44.16	0.59	3.46	< 0.10	0.44	0.08	0.16	< 0.10	0.12	< 0.02	< 0.02	< 0.03	< 0.03

The moulds were subsequently transferred in a furnace, maintained at 60 °C, and were left to cure in atmospheric pressure for three days. After the curing period, the samples were exposed to different conditions for a total of 42 additional days.

On the basis of exposure conditions, two conditions were chosen. The low temperature conditions included exposure of the samples to 60 ° C under confinement. The high temperature exposure was done in hydrothermal conditions, that in this study are defined as saturated steam pressures of 2 bars at 120° C.

The group of samples that was cured at 60 °C, was maintained in the moulds in the furnace for the rest of the curing period. The rest of the samples were removed from the furnace and left to cool down to room temperature for two hours before demolding.

For the hydrothermal conditions, pressure resistant glass bottles were used as autoclaves. Calculated amount of water, to generate saturated steam pressure of 2 bars at 120 °C, was inserted in the bottle prior to the samples' placement. The samples were placed in the bottles in pairs and were held in suspension from a thermocouple attached on the bottle's cap. Upon sealing, the bottles were placed

in a furnace maintained at 120 ° C. Pictures of the moulds used for exposure to 60 °C and 120°C can be found at Appendix 2 Figure B1 and B2.

On the basis of curing time, 6 groups of samples were obtained per curing temperature as the tests were performed at samples after 2, 3, 7, 14, 28, 42 days of curing. Prior to testing, the samples were left for two hours to cool down before demolding. Then they were cut on top and bottom to an final length of 50mm to achieve the parallel surfaces, necessary for the compression tests.

Table 4. Overview of the tests and analyses performed in this study (underlined and in bold the samples subjected to XRD, SEM and optical microscopy, the rest were subjected to uniaxial compressive tests)

Exposure time	**Exposure temperature**			
days	**60 ° C**	**120 ° C**	**60 ° C**	
2	3	3	6	# of samples tested for compressive strength
3	3	3	6	
7	3	3	6	
14	3	3	6	
28	3 **1 XRD + 1 thin section**	3 **1 XRD + 1 thin section**	6	
42	3	3	6	
Sample shape:	cylindrical	cylindrical	prismatic	

5.2 Experimental and analytical methods

X-ray diffraction

X-ray powder diffraction analyses were performed on two sample, one subjected to 28 days of curing at 60 ° C and another subjected to 28 days of curing at 120 ° C, in order to identify the crystalline phases formed. They were performed in Bragg-Brentano geometry with a Bruker D8 Advance diffractometer running at 40 kV and 40 mA. The diffractometer was equipped with a motorized slit with opening angle of 0.30°, primary and secondary soller slit of 2.5° and Lynxeye detector with opening angle of 2.94° and Ni-Kb filter. Data collection was carried out at room temperature using Cu Kα radiation (λ = 0.15406 nm) in the 2θ region between 10° and 120°, step size 0.015 degrees 2θ. The samples were deposited on a zero background holder (Si single crystal <510> wafer) and were rotated at 15 rpm during the measurement.

Phases were identified using the powder diffraction database from the International Centre for Diffraction Data (ICDD) and the Bruker search-match software EVA. Once phases were identified, the Bruker fitting programme TOPAS was used for quantification through Rietveld refinement. The

Rietveld method refines user-selected parameters to minimize the difference between the experimental pattern and a model based pattern simulated according to the presumed crystal and equipment parameters. It used to calculate the weight percentage of each crystalline phase and as a result, the amorphous content.

Optical Microscopy

Microstructure was assessed by polarization-and-fluorescence microscopy (PFM) at the age of 28 days. Polarizing and fluorescent microscopy is a two-fold integrated method, which allows the mineralogy and the internal structure of hardened porous materials to be characterized. In the present study, two thin sections were prepared by two samples exposed for 28 days to 60 and 120 ° C respectively.

Scanning Electron Microscopy - SEM

A FEI NovaNanoSEM 650 scanning electron microscope (SEM) was used to generate high-resolution micrographs of the micro-structures and perform quantitative spot chemical analyses on polished thin sections of two samples exposed for 28 days, one at 60 ° C and another at 120 ° C. The SEM operated at an acceleration voltage of 5 kV in low (40 Pa) vacuum mode to avoid charging of the non-conductive specimen. A gaseous analytical solid-state, back-scattered electron detector (GAD) was used for imaging both topographic and material contrast, while chemical composition was analyzed by a Noran micro analysis system (EDX).

Compressive strength tests

Uniaxial compressive strength experiments were performed at a constant loading rate of 72 kN/min on samples with an aspect ratio of 2. A total of 72 samples was tested mechanically. Three cylindrical samples per exposure age and per condition and 6 prismatic were tested to check reproducibility. The experiments were performed using a model Z250 Zwick – Roell testing machine to measure the deformation (stress – axial strain curves) of hydrated cement cylinders in unconfined conditions at room temperature, according to the API RP 10A [Recommended Practice for Testing Oil-Well Cements and Cement Additives, 2010] The failure strength was taken as the peak strength seen in the stress-strain curve

5.3 Results

5.3.1 Mineralogy – XRD data

The main hydration phases identified using XRD in the hardened cement samples after 28 days at 60 ° C, are the ettringite, portlandite and katoite (Table 5). All three phases are common hydration products of ordinary Portland cements with the standard Ca/Si ratio close to 3. On the other hand, C_3S and brownmillerite are cement clinker phases that have not completely reacted during hydration. Finally, the contained quartz in the sample has remained totally unreacted, as a result the amorphous content quantified in this case represents the C-S-H gel that forms during cement hydration. Thus, the main phase contained in the hardened cement pastes after a 28 days exposure at 60 ° C is the C-S-H gel.

Table 3. Phases identified by XRD analyses of hardened cement pastes with 40% quartz addition after 28 days of exposure at 60 ° C and 120 ° C.

Phase	Exposure temperature	
	60 ° C	120 ° C
Ettringite ($Ca_6Al_2(SO_4)_3(OH)_{12}\cdot 26H_2O$)	1,43%	-
Portlandite ($Ca(OH)_2$)	8,47%	-
Katoite ($Ca_3Al_2(SiO_4)1.5(OH)_6$)	3,45%	2,62%
C_3S (Ca_3SiO_5)	3,80%	-
Brownmillerite ($Ca_2(Al,Fe)_2O_5$)	7,72%	5,01%
Tobermorite ($Ca_{4.3}Si_{5.5}Al_{0.5}O_{16}(OH)_2 \cdot 4(H_2O)$)	-	10,4%
Afwillite ($Ca_3(Si_2O_4)(OH)_6$)	-	0,63%
α-C_2S hydrate ($Ca_2(SiO_3OH)(OH)$)	-	1,17%
Quartz (SiO_2)	26,21%	13,14%
Amorphous content	48,9%	67,1%

In the samples exposed to hydrothermal conditions for 28 days, the main hydration phases identified are the Tobermorite, α-C_2S hydrate and Afwillite. Afwillite is a hydration phase that has been reported to occur in cements with Ca/Si ratios of 1,5, α-C_2S hydrate forms at Ca/Si ratios close to 2, while Tobermorite at Ca/Si ratios around 1 (Hong and Glasser, 2004). Moreover, the quartz amount detected here is 50% less while the amorphous content is 37% more than in the sample exposed at 60 ° C (Fig. &). The fact that reaction products of different Ca/Si ratios coexist indicates that some of them are metastable reaction products as the system has not yet reached equilibrium. The high amount of amorphous content most probably represents both the C-S-H gel that forms initially upon hydration as well as dissolved quartz. The clinker phase C_3S, as well as the hydration products ettringite and portlandite, have been completely consumed at these conditions, while brownmillerite and katoite are detected in smaller amounts.

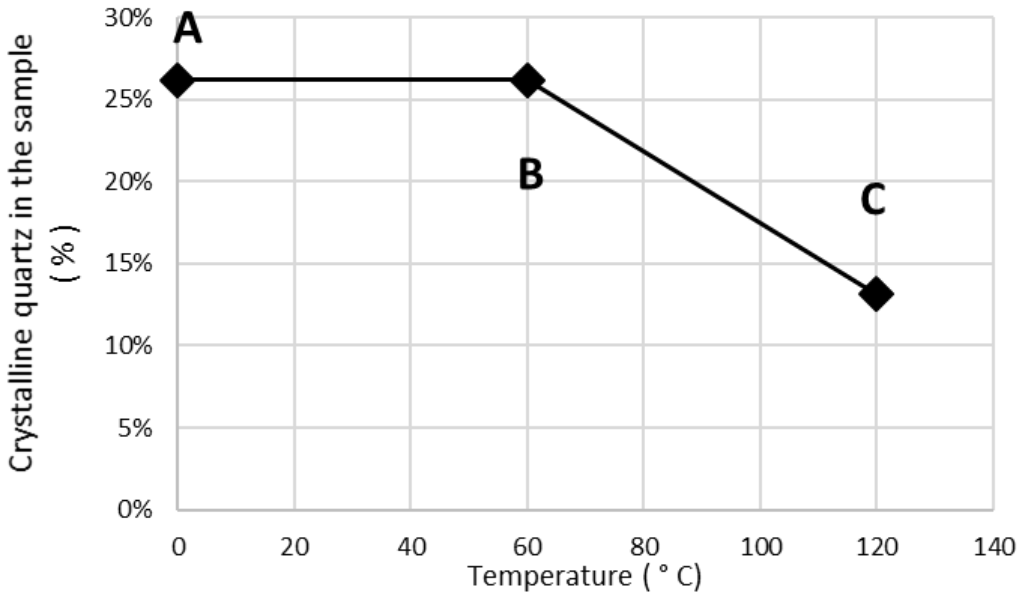

Figure 7. Percentage of crystalline quartz identified in the cement powder (A) and in the hardened cement pastes after 28 days of exposure at 60 ° C and at 120 ° C

5.3.2 Microstructure

5.3.2.2 Optical Observations

Optical microscopy examination of the samples showed a difference in the extend of hydration and the porosity between the samples exposed to the two different conditions. The sample exposed to 60 ° C (Figure 8a) shows some distinctive darker zones in the matrix dominated by the yellow fluorescent resin. The darker areas are spots where dense C-S-H cement grains dominate and prevent the fluorescent epoxy from impregnating indicating areas of lower capillary porosity. The yellow areas, where the epoxy impregnates deeper, represent areas with higher capillary porosity, where the porous C-S-H hydration products grew in the presence of higher amount of water and gave enough space to the hydration products to grow more porous structures. This local separation of water.is a phenomenon known in the cement science as microbleeding. Larger spherical pores are voids trapped during mixing. The white grains are the quartz grains. Their rims remain highly angular showing that they did not react at all.

In Figure 8 b and d show that the sample exposed to 120 ° C developed a capillary porosity more evenly distributed throughout the sample. Moreover, higher magnification images (Figure 8c) reveal precipitation of cement hydrates inside large pores.

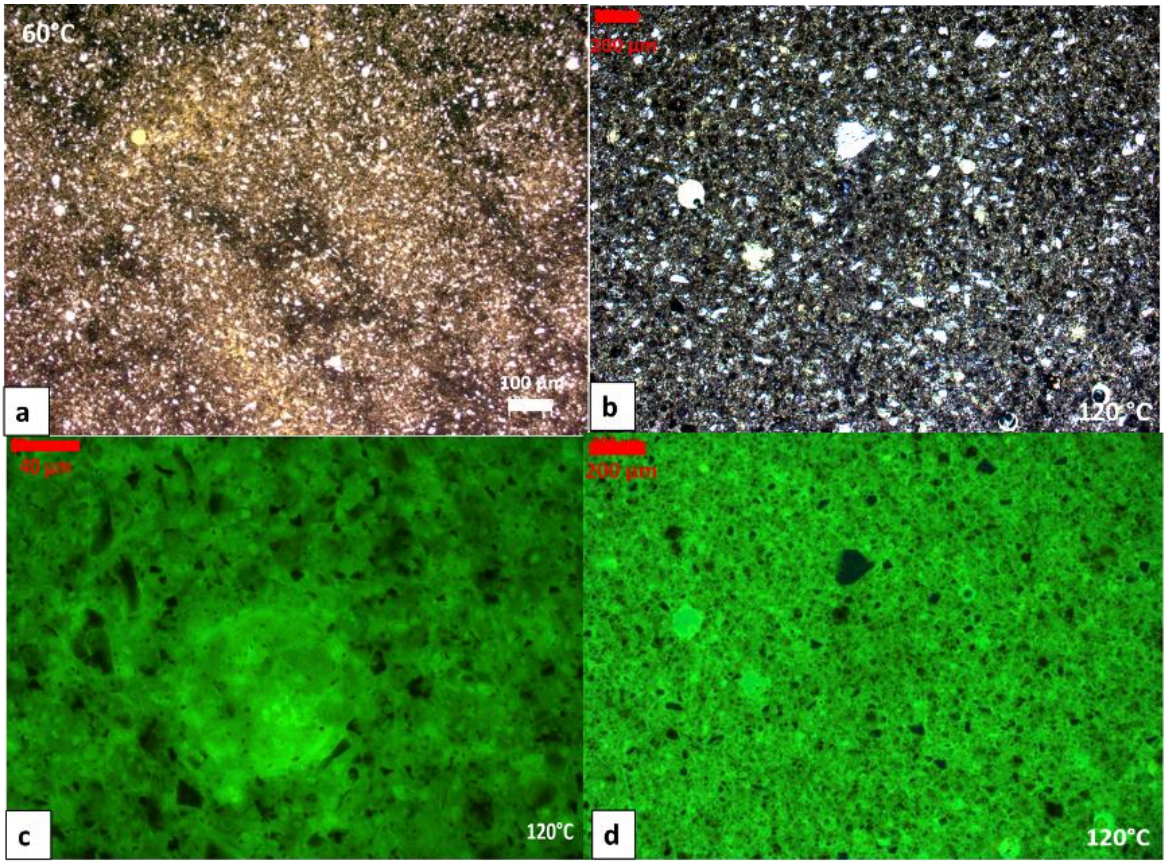

Figure 7. Microscope image of the hardened cement pastes under plain ultra-violet light (c, d)

5.3.2.1 SEM observations

SEM was used in order to observe the microstructure after 28 days of exposure of the hardened cement samples at 60 ° C and 120 ° C.

The hardened cement pastes exposed at 60 ° C are characterized by a very fine to amorphous matrix with areas of high and low porosity. At the 5-micrometer scale, the microstructure showed areas of highly porous and amorphous structures embeded with smooth-textured uniformly darker - grey areas. In the BSE images of Figure 8A-D, the highly heterogeneous microstructure of hardened cement paste can be observed. The porosity variations throughout the matrix are formed as a result of microbleeding. In the areas where more water was accumulated more porous C-S-H has hydrated as there was more space available. The denser C-S-H has hydrated in areas where the amount. The Microcracking was observed in images A, B, C to occur in the interface between densely hydrated and porous C-S-H.

BSE images of hardened cement pastes exposed to 120 ° C for 28 days can be seen in Figure 6 E-D. At the 5-micrometer scale the matrix appears very fine grained (Fig. 8 G) and the matrix seems to have a more homogeneous microstructure than the samples exposed to 60° C, as porosity seems the same throughout the sample. Moreover, the outer rims of the areas where C-S-H hydrates appear with a darker color due to the higher Si content, that indicates a reaction front between the C-S-H gel and the surrounding amorphous silica. The brighter spots in the inner areas of the C-S-H show Al and Fe enrichment. Well-formed Tobermorite crystals appear to grow inside the C-S-H gel (Figure 8 E ,F).

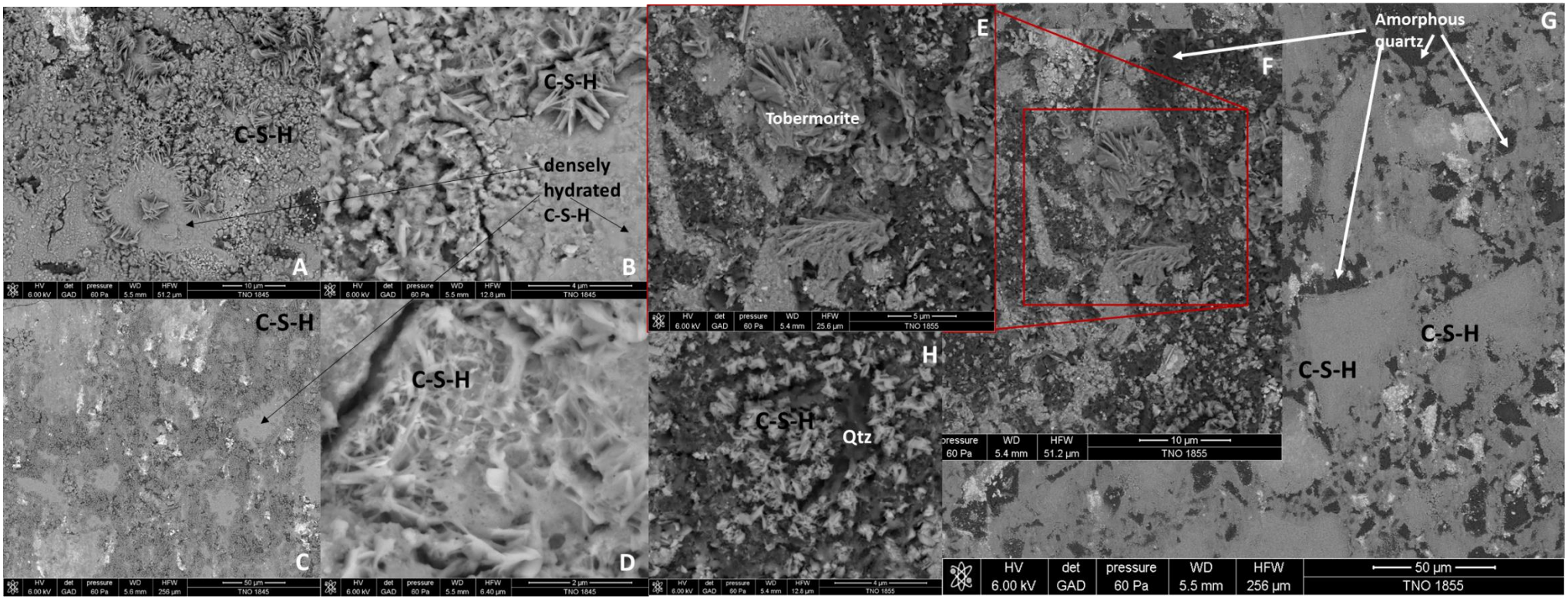

Figure 8. BSE images of SEM from hardened cement pastes after 28 days of exposure at 60 (A, B, C, D) and 120 C (E, F, G, H).

5.3.4 Mechanical data and strength

The mechanical data of the specimens were obtained by uniaxial compressive tests. The compressive strength, denoted as σ, was determined from the applied load at the point of sample failure. The term failure is defined here as the loss of strength beyond the maximum or peak strength. For each exposure age and condition, three samples were tested. Peak strength values fall in the range 29,36-50,32 Mpa, while standard deviations vary from 0,56 to 6,58 MPa (Table 6 and Figure 9 B). The highest average compressive strength values (50,32 MPa) were obtained by the cylindrical samples exposed to hydrothermal conditions for 42 days as seen in Table 6. Samples aged at 60 ° C exhibit a strength loss after the first 7 days of exposure, while samples exposed to hydrothermal conditions show a progressive strength gain throughout the examined period of 42 days. An additional series of standard prisms (40 mm x 40 mm x 160 mm) was aged at 60 ° C to check the accuracy of the compressive tests when performed in small cylinders (25 mm x 50 mm) against the prisms that are widely used by the cement industry. In Figure 2 B, the test shape conversion factors from that can range from 0.65 to 0.9 (Vandegrift and Schindler, 2006) of the prisms' values are plotted. The area between the two black dashed lines represents the field where with respect to the prisms' values (yellow line), the values of the cylindrical test samples of the same age and exposure conditions (blue line) should be plotted in.

Table 4 . Average uniaxial compressive strength values of samples tested

	Compressive strength (MPa)					
Exposure age	60 ° C cylinders	stdv	120 ° C cylinders	stdv	60 ° C prisms	stdv
2 days	29.36	0.56	34.29	5.20	43.79	491
3 days	39.83	3.66	36.16	5.33	45.00	5,91
7 days	42.03	4.92	42,.08	1.93	46.61	1.69
14 days	35.69	3.86	42.27	6.57	39.69	3.49
28 days	34.24	6.26	38.45	7.60	38.25	6.58
42 days	30.28	1.64	50.32	1.64	45.44	4.00

Young's modulus, denoted as E, was calculated from the initial linear portion of the stress versus strain curves. E values range from 20 to 42,42 GPa, with peak values in the range of 40 to 42 GPa and standard deviations have a maximum of 4 GPa for the samples aged at 60 ° C and a maximum of 6 GPa for the samples exposed to hydrothermal conditions (Table 7). Samples aged at 60 ° C reached their maximum values after 3 days of exposure and started losing stiffness up until the 14th day of exposure. On the contrary, samples aged at hydrothermal conditions reached their peak values at 42 days of

exposure. All samples, regardless exposure conditions, exhibit a substantial loss of stiffness in the period between the 3 and 14 days (Figure 9C).

Table 7. Average values of E modulus of samples tested

Exposure age	E modulus (GPa)			
	60 ° C cylinders	stdv	120 ° C cylinders	stdv
2 days	20.07	4.15	35.12	0.27
3 days	40.85	1.35	39.37	2.11
7 days	36.97	3.14	32.15	1.43
14 days	21.75	3.46	31.71	0.25
28 days	24.38	2.78	36.14	6.15
42 days	32.13	2.60	42.42	5.93

While after the 14 days all samples show a recovery, samples exposed to hydrothermal conditions regain and exceed the initial high values. The stress – strain curves were characterized by an initial elastic part followed by a sharp loss of strength (failure).

The failure was characterized by abrupt brittle fracturing, with fractures developing across the axial directions (column – like) while the shear cone was formed on the contact surfaces between the test sample and the steel plates (Figure 8 D).

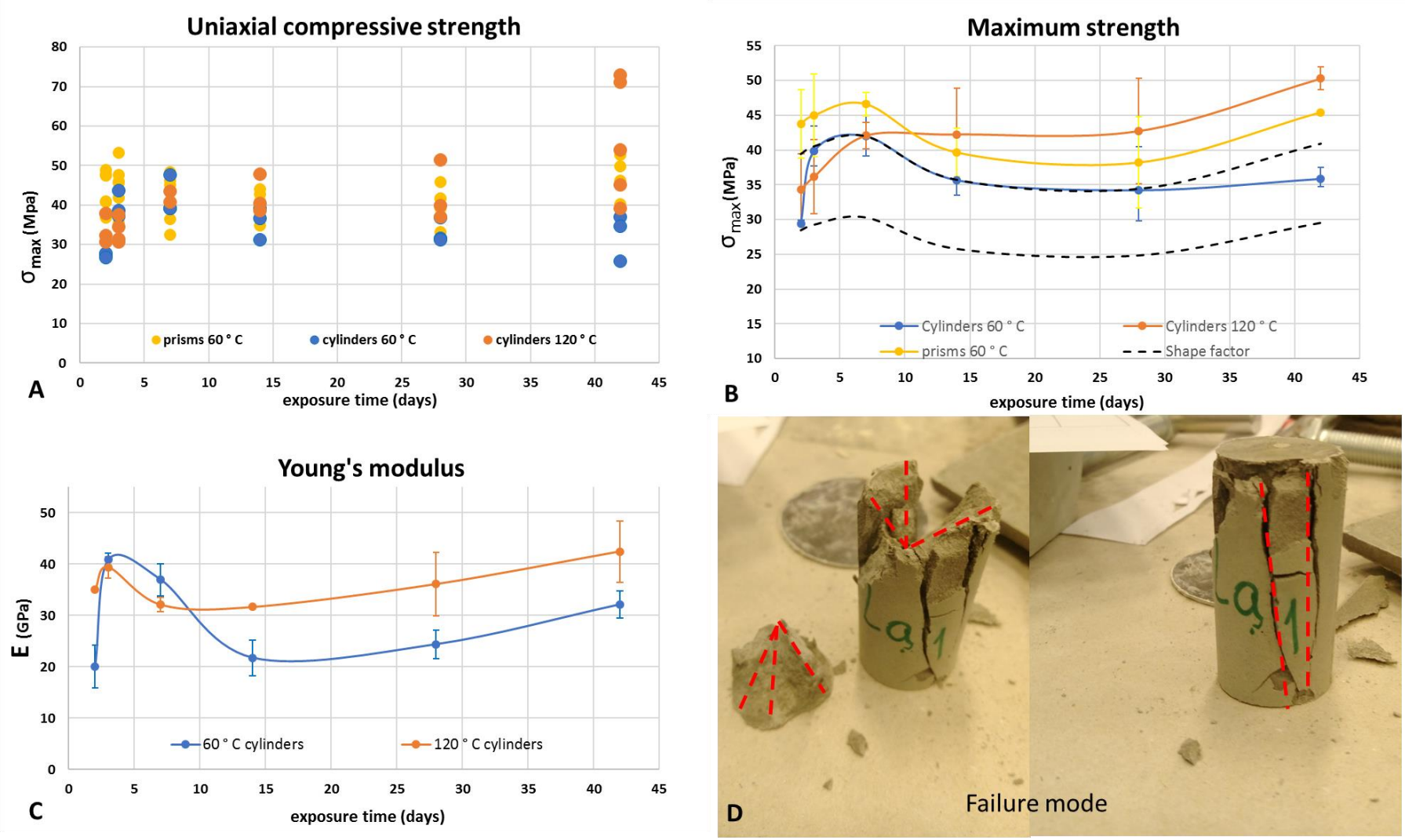

Figure 8. Mechanical data of hardened cement pastes as obtained by uniaxial compressive tests. Cylindrical samples exposed to 60 ° C (blue) and 120 ° C (red), standard prisms exposed to 60 ° C (yellow).

6. Discussion

6.1 Present experiments

For the experiments in this study two exposure temperatures were selected 60 and 120 ° C. The first temperature corresponds to the average wellbore temperature during cementing operation while the second was chosen to investigate the performance of this formulation above the temperature where strength retrogression occurs. This temperature of 60 ° C is obtained with fluid recirculation in the well, that is being maintained for approximately a month after cement placement. After 28 days the hardened cement gains 66% of its final strength, meaning that the cement sheath will have enough strength to support the steel casing and withstand the operation induced stresses. Taking this into account, the XRD and microstructural analyses were performed at samples exposed to each temperature for 28 days, assuming that at that time they will have the exact mineralogy and microstructure as the cement sheath by the time the operation restarts.

Mineralogy

According to the XRD analyses, the hydration products at 60 ° C are the C-S-H gel, Portlandite, Ettringite and Katoite as the main aluminium bearing hydration phase. C_3S and Brownmillerite are both clinker phases and their presence after 28 days indicates that hydration was incomplete. Moreover, the amount of quartz detected in the sample indicates that the silica flour addition did not react at all in the sample exposed to 60 ° C. As a result, the silica flour addition at this temperature acts as a filler and the special high temperature formulation is nothing more than a regular type G cement with a higher water to cement ratio and a quartz flour filler. The conditions we conducted these experiments (60 ° C and 28 days of exposure) directly correspond to the temperature and time of in-situ ageing of the cement sheath before the well becomes operational again. Therefore, this suggests that the same will apply for the cement sheath in the wellbore. The mineralogy of the cement sheath will be the same as the one of type G oilwell cement with 40% quartz filler, since during the period of in- situ ageing the temperature in the well is not high enough to allow quartz reaction.

When exposed to 120 ° C for the same period, the main hydration products are Tobermorite and Katoite with minor phases being Afwillite and α-C_2S hydrate. The mineral Afwillite has a Ca/Si of 1.5, is associated with hydrothermal curing, and has been reported to occur metastably below 200 ° C (Taylor, 1990), α-C_2S hydrate has a Ca/Si of 2 while Tobermorite has a Ca/Si of 0.8 to 1. The coexistence of these three crystalline phases suggests that some of them occur metastably at this age and temperature. Moreover, only 50% of the initial quartz was detected in this sample indicating that even at saturated steam pressures after 28 days the overall active Ca/Si composition of the hardened cement paste is around 1.5 and not 1 as the 40% addition of silica flour was aiming to.

Microstructure

The matrix of the sample exposed to 60 ° C appeared to be highly inhomogeneous, having areas were cement was densely hydrated and parts were porous C-S-H was formed. When exposed to 120 ° C the larger voids, that formed by air entrapment during mixing, were being filled through precipitation of hydrates while the porosity appeared lower compared to the samples aged at 60 ° C while no distinctive porosity variations (microbleeding) were detected. The different microstructure of the 120° C is a result of more extensive hydration occuring at this temperature, as no clinker phases were detected. Moreover, at this temperature the quartz reacted with the cement phases forming less porous minerals like Tobermorite, that were precipitated throughout the matrix causing a further refinement of the porosity.

Moreover, another type of heterogeneity could be detected macroscopically, as the samples have a different color on the top (darker) than the bottom (Appendix 2 Figure B3). This color gradient is present in the samples regardless of exposure temperature, thus it could have been caused by a particle segregation during the slurry setting period (first 3 days) during which all samples were kept at 60 ° C. The slurry consists of cement and quartz particles that have different sizes, so upon hydration two types of particles will be formed, the cement hydrates and the quartz particles that will remain unreactive at the setting temperature. These two particle types have different densities and, as the solidification does not occur instantaneously, the heavier can be drawn to the bottom of the sample forming a density gradient along the sample. This particle segregation, although it was not observed in the microscopic study, when extrapolated in a cement sheath scale, could generate significant heterogeneities in the porosity and overall microstructure of the cement sheath with detrimental implications on the mechanical behavior of the wellbore.

Mechanical properties

The experimental procedure of this study included multiple uniaxial compressive tests at cylindrical and prismatic samples, at different ages of exposure. In order to determine if there is an effect of shape on the obtained strength values, as our values were obtained from cylindrical samples while the standard tests practices refer to cubic values, an additional series of tests was performed on prismatic samples exposed to 60 ° C.

As seen in Figure 9 B, all series exhibit a strength gain up until the 7^{th} day. They exhibit a different behaviour at the 14^{th} day, where the series exposed to 60 ° C lose almost half of the initially gained strength and maintain it until the 42 days while the series exposed 120 ° C keep gaining strength up until the 42 days. The strength results can be explained when combined with the mineralogy and microstructure analyses performed at the samples at 28 days. The hardened cement pastes exposed to 120 ° C consist of more crystalline phases and have a more homogeneous pore structure due to the precipitation of hydrates. Unlike the 60 ° C series, the 120 ° C series continues to gain strength after

the 28 days, gaining an additional 18% the last two weeks of exposure. This increase in strength is related to the formation of more crystalline minerals due to the reaction of quartz at this temperature, to complete hydration of the clinker minerals and to the further precipitation of hydrates inside large pore that results in a refinement of the matrix.

The lower and higher cube to cylinder shape conversion factors are plotted with black dashed lines in Figure 8 B. As indicated, the measured cylindrical values (blue line) follow the 0,9 conversion factor line or fall into the area of the anticipated values and they follow the same trend. It is therefore safe to assume that the measured cylindrical values of the 120 ° C series can be accurately converted to cubic values.

In terms of stiffness (Figure 8 C), both series show an increase with time but the 120 ° C series show much higher values. The 60 ° C series has an overall increase of 60% (from 20 to 32 GPa) while the 120 ° C series of 21% (from 35 to 42 GPa). Our results agree with previous studies (Roy, 1987) where cement formulations with silica additions show increasing magnitudes for the Young's modulus with increasing temperature. Nevertheless, the values measured are considerably high especially when compared to plain type G cement that shows a stiffness loss with increasing temperature until the temperature of 120 ° C (Odelson, Kerr and Vichit-Vadakan, 2007).

6.2 Comparison with related studies

The American Petroleum Institute (API) has set 7 MPa as the minimum compressive strength required in order for cements to be used as sealants for very deep oil or geothermal wells (API Specification 10A, 2010). Characterization of cement formulations' mechanical performance by means of compressive strength is a common practice in the cement industry. However, recent studies have shown cement suitability assessment based solely on the maximum compressive strength to be insufficient mainly for two reasons. First, Ghabezloo *et al*,(2008) examined the mechanical behavior of hardened cement paste under isotropic loading in drained, undrained and unjacketed conditions and through the results obtained, were able to prove that "the behavior of hardened cement paste can be described within the framework of porous media". Porous media characterization requires the pore fluid pressure to be accounted for, especially in conditions where the material encounters high pressure and/or temperature, (like in the case of HPHT geothermal wells) but in standard uniaxial compressive tests the effects of pressure and temperature are neglected. As a result, the accurate state of effective stress cannot be estimated. Second, the tensile stresses developed in the cement-casing interface, by the internal pressurization and thermal effects (casing expansion-contraction), have more detrimental effects on the cement sheath integrity than the compressive ones (Philippacopoulos and Berndt, 2001, 2002; Lavrov and Torsæter, 2016). Thus, the tensile strength of

the cement sheath is a more crucial element in the assessment of the cement sheath mechanical behavior than the compressive one currently used.

The performance of a porous material that is exposed to loading variations can be described by its constitutive law, failure criteria and initial state of effective stress. Since cement performs as a porous material (Ghabezloo *et al.*, 2008), its mechanical behavior can be described by poro-mechanics laws and its constitutive laws and failure criteria can be determined by triaxial tests that are the standards in rocks mechanics. Following this approach and with use of methodology applied in rocks mechanics, recent studies (Ghabezloo, Sulem and Saint-Marc, 2009; Sakai and Kishi, 2017) have given some more complete insights on the mechanisms that cause the HCP deformation.

Sakai and Kishi, (2017) investigated the deformation of HCP (class G cement) of different saturation degrees, under confining pressure. They noticed that the failure pattern changed from brittle to ductile with increasing confining pressure and moisture content. This means that the higher the moisture contents, the lower the value of the confining pressure that can cause macroscopic damage. The ductile failure is proposed to be governed by climb-controlled dislocation motion, that occurs when crystal defects, or dislocations, move under confining pressure because of the energy produced by the crystal structure deformation. The dislocations are suggested to form in Portlandite, the calcium hydroxide, during drying shrinkage. Dislocation accumulation that causes strain hardening and leads to brittle behavior is avoided by the presence of water that accelerates the dislocation removal. Moreover, when samples were saturated with sucrose solution, calcium hydroxide precipitation was suppressed and the deformation became more brittle indicating that, in water saturated samples the mechanism of pressure solution was acting in parallel with dislocation climb.

Although this study was performed on class G cement samples, as opposed to the cement formulation with 40% silica used in our study some comparison can be held in terms of deformation mechanisms. The microstructural results of our study indicated that exposure in higher temperatures promotes hydrates precipitation in the pores. This results in decreased porosity, higher Young's modulus, decreased permeability as well as in lower amount of free water present in the sample compared to a plain class G cement. The decrease of free water with increasing temperature, and subsequently increasing confining pressure, will probably result in a more brittle response of this cement with increasing confining pressure. This is due to the lower amount of water present on a sample exposed to higher temperatures, which could facilitate accumulation of dislocations due to strain hardening that could result in brittle failure. Moreover, after exposure to 120 °C and 2 bars for 28 days, the Portlandite formed upon cement hydration has completely reacted with the available quartz and water to form more C-S-H. This means that the proposed mechanism of dislocations forming in

Portlandite during drying shrinkage, could not act on this cement. An alternative mechanism of dislocations formation should act in this system.

The above mentioned work the deformation of hardened cement pastes by Sakai and Kishi, (2017) does not take under consideration high temperatures that are encountered in geothermal wells. Ghabezloo, Sulem and Saint-Marc(2009) investigated the HCP mechanical response to rapid temperature changes by performing undrained heating tests with heating –cooling cycles. The purpose of the study was to evaluate the effect of pressure, induced by the pore fluid, on volume change during undrained deformation. This phenomenon, is known in poro-mechanics as "thermal pressurization of the pore fluid" and is caused due to the different thermal expansion coefficients of the solid matrix phase and the pore fluid. When temperature increases the pore fluid expands, inducing a pressure towards the solid phase that causes a reduction of the effective mean stress, which could potentially cause failure or hydraulic fracturing of the medium. The increase of pore fluid pressure per unit temperature increase is called "thermal pressurization coefficient" (Λ) and its value varies from 0.01 to 1.5 MPa/°C (Ghazebloo and Sulem, 2009), depending on the material, the temperature change and the state of stress. According to the results, the pore fluid pressure changes linearly with temperature changes and is described by a constant thermal pressurization coefficient equal to 0.6 MPa/°C. Additionally, the results of the undrained test recorded some variations on the thermal expansion of cement pore fluid during the heating cooling phases. It was recorded that the thermal expansion of pore fluid was larger than the one of pure bulk water and that the rate of its increase with temperature was smaller. This phenomenon was attributed the different thermal behavior of water, when it is confined in pores, and in to the presence of dissolved ions in the cement paste pore fluid.

Again, even though the findings of the above mentioned study refer to class G cement, it offers a useful guideline on the approach that should be followed in order to investigate and assess the mechanical behavior of different cement formulations on with temperature changes. Moreover, this approach could serve as a screening step when new formulations for high temperature applications are developed. On the other hand, when the exact mechanical behavior of a cement formulation is investigated this methodology would be insufficient and should be followed by more rigorous tests as described in the next section.

6.3 Future Work

An attempt to predict cement sheath failure under high temperature would essentially require to predict the mechanical behavior of the system formation-cement sheath-steel casing. In order for their mechanical behavior to be modeled the following should be determined:

•The coefficients of thermal expansion of cement and rock;

• The thermal and elastic properties of cement, steel casing and rock;

• The compressive as well as tensile strengths of cement;

•The cement shrinkage during setting and the initial stresses in the cement sheath;

The studies by Ghabezloo, Sulem and Saint-Marc(2009) and Sakai and Kishi, (2017) on the cement wellbore mechanical behavior with pressure and temperature variations were performed on type G cement although currently HPHT geothermal operations use type G cement with 40% silica addition. Even though the methods used in our study highlighted important differences between the properties of the two cement formulations more properties such as the porosity and permeability of the cement class G + 40% silica should be determined in order to be able to use the existing studies on plain class G cement and draw conclusions/ predict its performance with pressure and temperature variations. A special attention should be given in choosing the age and the exposure conditions of the hardened cement samples to perform the experiments on. These parameters are essential as cement physical properties change significantly with age and the conditions under which it took place. It is suggested to:

a. estimate the shrinkage, porosity and permeability
b. calculate the initial state of stress,
c. perform triaxial tests suggested below

on samples aged for 28 days at 60 °C, as these conditions more accurately represent the conditions of cement sheath in-situ ageing. Subsequently, it is suggested to study the mineralogy and microstructure of samples exposed to hydrothermal conditions after having initially aged for 28 days at 60°C Another step should include investigation of the mineralogical changes of cement + silica formulations after cycles of exposure to high (< 450 °C) and low (60 ° C) temperatures in order to determine the extent of Portlandite consumption/ reaction with increasing temperature in the presence of silica.

In a next stage, triaxial tests should be performed in order to determine whether the mechanism controlling the mechanical response of the cement+ silica sealant is the same as with the type G cement (dislocation glide). This could be done by performing stepwise creep tests at different confining pressures to determine the creep mechanism (diffusion creep, dislocation creep or

dislocation climb) or the creep mechanism changes occurring with increasing differential stress. Moreover, they could be combined with monotonic triaxial tests with constant displacement rate at different confining pressures. The obtained stress-strain curves could be used in order to define the conditions where the transition from brittle to ductile deformation occurs.

This should be followed by macroscopic investigation of the mechanically tested samples in order to verify the failure mode the test results would indicate. Subsequent microscopic investigation on mineralogy and microstructure variations between mechanically tested samples and untested samples of the same cement formulation would provide an insight on the transport mechanisms that acted on the samples upon increasing confining pressure.

In the final stage, drained, undrained and unjacketed triaxial tests should be performed under isotropic loading in order to determine the tested cement's bulk modulus properties. Finally, undrained heating tests with heating-cooling cycles, performed at the high temperatures (<400 ° C) encountered by HPHT geothermal operations, are suggested. Through these tests it would be possible to determine the thermal expansion coefficient of the cement and the cement pore fluid, its variations at very high temperatures and whether they are anomalous or result in a constant thermal pressurization coefficient of the cement paste. If a constant thermal pressurization of the cement paste is derived, it could be used, together with the above mentioned bulk properties of the cement, in the Eq.1 to calculate the diffusion of pore fluid pressure in the sample (or cement sheath) and the subsequent pressure difference that would remain in the sample (or cement sheath). This pressure difference could be then used to estimate the effective stress of the cement sheath and predict, this way, its mechanical response to the stresses applied by the steel casing and/or the formation.

7. Conclusions

This study has addressed the mineralogical and mechanical changes occurring at cement during ageing at different in–situ conditions and their implications on the mechanical degradation of the cement sheath of a HPHT geothermal wellbore. A review of what is known on the impact of HPHT ageing conditions and HPHT production stresses on cement sheath mineralogy and mechanical behavior, has been presented as background. Additionally, experiments have been performed with the aim of assessing the adequacy of the standard durability estimation methods to reliably evaluate the performance of this cement formulation at low and high temperatures. Methods employed included XRD, SEM and optical analyses of the mineralogy and microstructure, as well as uniaxial compressive strength tests applied to samples cured for 28 days at 60 ° C and 120 ° C- 2 bars. The review demonstrated that previous work has only investigated the deformation mechanisms of class G cement paste under temperature as high as 50 ° C, while no related study has been performed on the special cement formulation that is used on construction of HT geothermal wellbores. Nevertheless, these studies provide a useful guideline on the testing methodology, that should be followed to study the mechanical behavior of cement formulations aimed for use in HPHT geothermal operations.

Present results obtained for samples exposed to 60 ° C for 28 days led to the following conclusions:

1. The compressive strength values obtained by the 25x50mm cylinders fall into the anticipated range (0,65 to 0,9 of the prisms (4x4x16 cm)) and follow the same trend as the standard prisms used by the industry. The obtained values for cylindrical samples can be accurately converted to the cubic value when divided by the conversion value

2. When the curing of the cement sheath takes place at temperature as high as 60 ° C, the quartz does not react at all. As a result, the hardened cement gains early strength but loses almost 19% of it in the first 28 days.

3. The mineralogy, microstructure and subsequently the compressive strength of the cement sheath are similar to the ones of a plain type G cement with 40% quartz filler. The silica-rich phases such as Tobermorite and Xonotlite, this cement formulation is aimed to develop, have not been formed thus the compositional and mechanical potential of it has not been reached by the moment the wellbore becomes operational again.

Results obtained for samples exposed to 120°C for 28 days led to the following conclusions:

4. After 28 days of exposure at 120°C, only 50% of the added quartz has reacted, resulting to an active C/S of 1.5-2. This means that the Ca-rich phases that cause cement strength retrogression are still present. The co-existence, at this age, of phases with different C/S ratio

indicates that equilibrium has not been reached/(or that their presence is metastable). The fact that at 42 days of exposure samples gain an additional 31% of their strength indicates that more quartz reacted and more Tobermorite was formed.

5. Filling of the pores by mineral precipitation at higher temperature contributes to the increase of the peak compressive strength and increased Young's modulus.
6. The approach, followed by the industry to assess cement formulations for HTHP geothermal applications by autoclaving them upon hydration, does not accurately represent the conditions of in-situ ageing of a wellbore cement sheath

Implications for cement sheath:

7. The mineralogy, initial state of stress, porosity and permeability of the cement sheath when it is exposed to production induced P, T stresses, are these of a HCP exposed to 60 °C for 28 days.

8. The present experiments showed that exposure to higher temperatures increases the stiffness of the HCP (Figure 9B, Table 7). High stiffness of the sealant indicates a slower and more brittle mechanical response of the cement sheath to the expansion and contraction of the steel casing and increases the probability of cement sheath shear failure.

9. Upon operation where the T increases, the cement formulation studied here, has the compositional potential to further continue hydration (assuming a tight confinement where there will be no water loses). But as T increases so does the stress field acting on the cement sheath. As a result, the precipitation of new phases will take place in parallel with deformation. Future work should focus on understanding how these mechanisms act on the specific cement formulation, at high temperature (<.400°C) and high confining pressure.

10. The methods used in this study can serve as a stepping stone when the aim is to develop new cement formulations with specific properties. However, when the aim is to determine their performance on HPHT conditions, more properties should be determined. Knowing the porosity and permeability of the investigated formulation would allow a first comparison with the standard (class G) cement. Complete evaluation of a sealant's performance under HPHT conditions requires determining its coefficients of thermal expansion, its thermal and elastic properties, its tensile and compressive strengths and its initial state of effective stress.

Acknowledgments

The present study was a part of EU project GEOWELL and was conducted in collaboration with TNO.

I would like to thank prof. dr. Chris Spiers and prof. dr. Hans de Bresser for their help and support during this project. Furthermore, I would like to thank dr. Ir. Penny Pipilikaki for her invaluable mentoring and guidance throughout this study, the helpful reviews and discussions of ideas. Finally, I would like to thank Efi, Vasili, Greta, Nasia and Francesco for their endless patience and love during this period.

Appendix 1

Table A1 a. API cement classification based on physical and performance requirements

Well cement class				A	B	C	D	G	H
Mix water, % mass fraction of cement (Table 5)				46	46	56	38	44	38
Fineness tests (alternative methods) (Clause 6)									
Turbidimeter (specific surface, minimum, m^2/kg)				150	160	220	NR[a]	NR	NR
Air permeability (specific surface, minimum, m^2/kg)				280	280	400	NR	NR	NR
Free-fluid content, maximum, percent (Clause 8)				NR	NR	NR	NR	5,9	5,9
Compressive strength test (8 h curing time)	**Schedule number** Table 6	**Final curing temperature** °C (°F)	**Curing pressure** MPa (psi)	**Minimum compressive strength** MPa (psi)					
(Clause 9)	NA[b]	38 (100)	atm.	1,7 (250)	1,4 (200)	2,1 (300)	NR	2,1 (300)	2,1 (300)
(Clause 9)	NA	60 (140)	atm.	NR	NR	NR	NR	10,3 (1 500)	10,3 (1 500)
(Clause 9)	6S	110 (230)	20,7 (3 000)	NR	NR	NR	3,4 (500)	NR	NR
Compressive strength test (24 h curing time)	**Schedule number** (Table 6)	**Final curing temperature** °C (°F)	**Curing pressure** MPa (psi)	**Minimum compressive strength** MPa (psi)					
(Clause 9)	NA	38 (100)	atm.	12,4 (1 800)	10,3 (1 500)	13,8 (2 000)	NR	NR	NR
(Clause 9)	4S	77 (170)	20,7 (3 000)	NR	NR	NR	6,9 (1 000)	NR	NR
(Clause 9)	6S	110 (230)	20,7 (3 000)	NR	NR	NR	13,8 (2 000)	NR	NR
Thickening-time test	**Specification test schedule number** Tables 9 through 11	**Maximum consistency** (15 min to 30 min stirring period) B_c[c]		**Thickening time** (minimum/maximum) min					
(Clause 10)	4	30		90[d]	90[d]	90[d]	90[d]	NR	NR
(Clause 10)	5	30		NR	NR	NR	NR	90[d]	90[d]
(Clause 10)	5	30		NR	NR	NR	NR	120[e]	120[e]
(Clause 10)	6	30		NR	NR	NR	100[d]	NR	NR

[a] NR indicates "no requirement".

[b] NA indicates "not applicable".

[c] Bearden units of consistency, B_c, obtained on a pressurized consistometer as defined in Clause 10 and calibrated in accordance with the same clause.

[d] Minimum thickening time.

[e] Maximum thickening time.

Table A1 b. API cement classification based on chemical requirements

	Cement class					
	A	B	C	D	G	H
Ordinary grade (O)						
Magnesium oxide (MgO), maximum, percent	6,0	NA[a]	6,0	NA	NA	NA
Sulfur trioxide (SO_3), maximum, percent[b]	3,5	NA	4,5	NA	NA	NA
Loss on ignition, maximum, percent	3,0	NA	3,0	NA	NA	NA
Insoluble residue, maximum, percent	0,75	NA	0,75	NA	NA	NA
Tricalcium aluminate (C_3A), maximum, percent[3]	NR[c]	NA	15	NA	NA	NA
Moderate sulfate-resistant grade (MSR)						
Magnesium oxide (MgO), maximum, percent	NA	6,0	6,0	6,0	6,0	6,0
Sulfur trioxide (SO_3), maximum, percent[b]	NA	3,0	3,5	3,0	3,0	3,0
Loss on ignition, maximum, percent	NA	3,0	3,0	3,0	3,0	3,0
Insoluble residue, maximum, percent	NA	0,75	0,75	0,75	0,75	0,75
Tricalcium silicate (C_3S) maximum, percent[d]	NA	NR	NR	NR	58	58
minimum, percent[d]	NA	NR	NR	NR	48	48
Tricalcium aluminate (C_3A), maximum percent[d]	NA	8	8	8	8	8
Total alkali content, expressed as sodium oxide (Na_2O) equivalent, maximum, percent[e]	NA	NR	NR	NR	0,75	0,75
High sulfate-resistant grade (HSR)						
Magnesium oxide (MgO), maximum, percent	NA	6,0	6,0	6,0	6,0	6,0
Sulfur trioxide (SO_3), maximum, percent[b]	NA	3,0	3,5	3,0	3,0	3,0
Loss on ignition, maximum, percent	NA	3,0	3,0	3,0	3,0	3,0
Insoluble residue, maximum, percent	NA	0,75	0,75	0,75	0,75	0,75
Tricalcium silicate (C_3S) maximum, percent[d]	NA	NR	NR	NR	65	65
minimum, percent[d]	NA	NR	NR	NR	48	48
Tricalcium aluminate (C_3A), maximum, percent[d]	NA	3	3	3	3	3
Tetracalcium aluminoferrite (C_4AF) plus twice the tricalcium aluminate (C_3A), maximum, percent[3]	NA	24	24	24	24	24
Total alkali content expressed as sodium oxide (Na_2O) equivalent, maximum, percent[e]	NA	NR	NR	NR	0,75	0,75

[a] NA indicates "not applicable".

[b] When the tricalcium aluminate content (expressed as C_3A) of the cement is 8 % or less, the maximum SO_3 content shall be 3 %, or 3,5 % for class C cement.

[c] NR indicates "no requirement".

[d] The expressing of chemical limitations by means of calculated assumed compounds does not necessarily mean that the oxides are actually or entirely present as such compounds. The compounds are calculated according to the ratio of the mass percentages of Al_2O_3 to Fe_2O_3, where w is the percentage mass fraction of the compound indicated in the subscript:

— When $w_{Al_2O_3}/w_{Fe_2O_3}$ is greater than 0,64, the compounds shall be calculated as follows:

$C_3A = 2,65 \times w_{Al_2O_3} - 1,69 \times w_{Fe_2O_3}$

$C_3S = 4,07 \times w_{CaO} - 7,60 \times w_{SiO_2} - 6,72 \times w_{Al_2O_3} - 1,43 \times w_{Fe_2O_3} - 2,85 \times w_{SO_3}$

$C_4AF = 3,04 \times w_{Fe_2O_3}$

— When $w_{Al_2O_3}/w_{Fe_2O_3}$ is 0,64 or less, the C_3A content is zero.

— The C_3S and C_4AF shall be calculated as follows:

$C_3S = 4,07 \times w_{CaO} - 7,60 \times w_{SiO_2} - 4,48 \times w_{Al_2O_3} - 2,86 \times w_{Fe_2O_3} - 2,85 \times w_{SO_3}$

$C_4AF = 3,04 \times w_{Fe_2O_3}$

[e] The sodium oxide equivalent, expressed as Na_2O equivalent, shall be calculated by the formula:

Na_2O equivalent is equal to $0,658 \times w_{K_2O} + w_{Na_2O}$.

Appendix 2

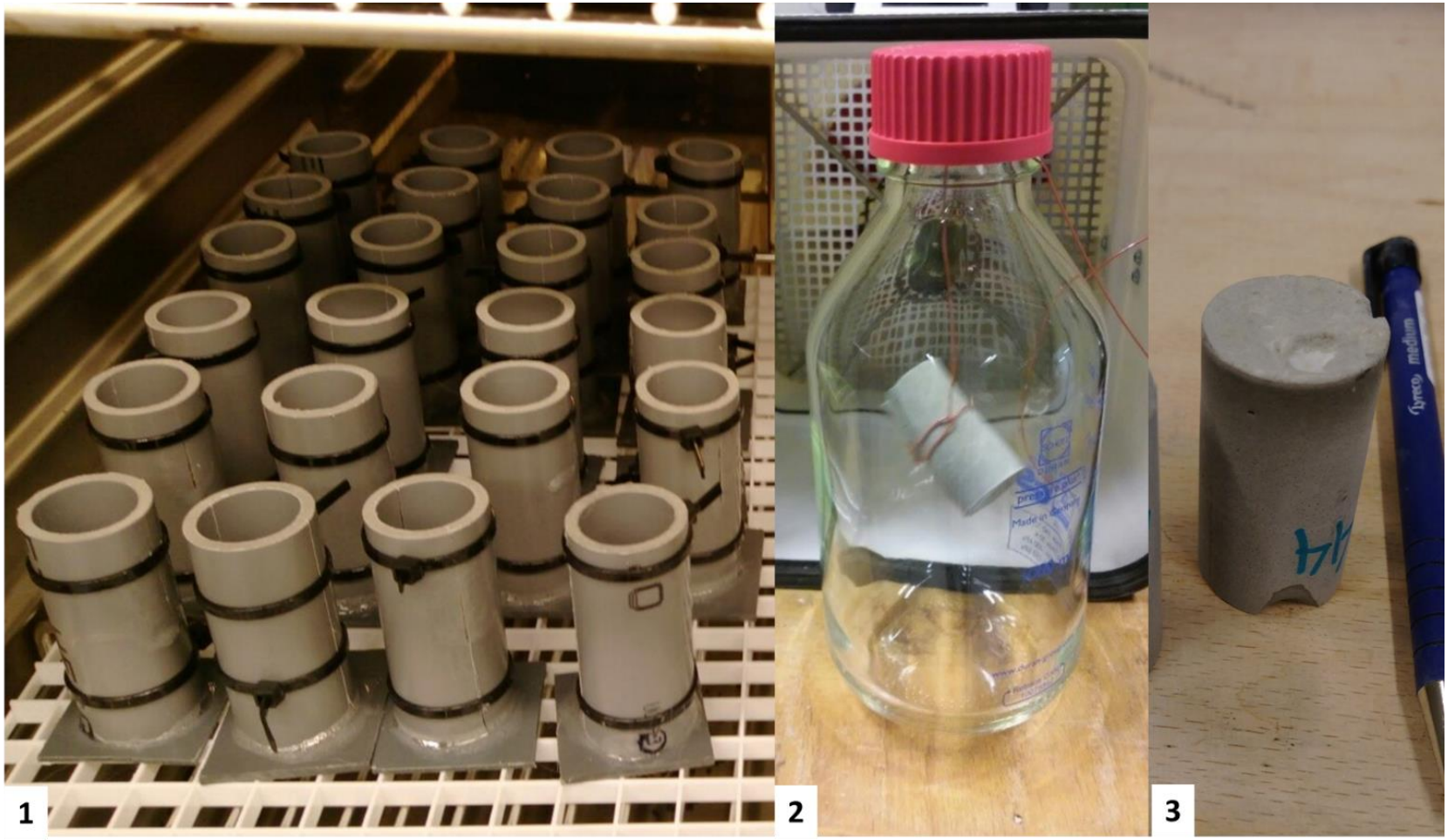

Figure B. Picture of moulds used for setting and exposure to 60 C (1), picture of temperature and pressure resistant glass bottles used for exposure to 120 C (2) and picture of sample showing a colour gradient from top to bottom (3)

References

API Specification 10A (2010) *Specification for Cements and Materials for Well Cementing*. 24th edn, *American Petroleum Institute*. 24th edn. API Publishing Services, 1220 L Street, NW, Washington, DC 20005.

Dobson, P. *et al.* (2017) 'Supercritical Geothermal Systems -A Review of Past Studies and Ongoing Research Activities', in *PROCEEDINGS, 41st Workshop on Geothermal Reservoir Engineering*.

Dusseault, M.B., Gray, M.N., Nawrocki, P. a, 2000. Why oilwells leak: Cement behavior and long-term consequences, in: SPE International Oil and Gas Conference and Exhibition, SPE 64733. p. 8. doi:10.2118/64733-MS

Fridleifsson, I. B. (2001) 'Geothermal energy for the benefit of the people', *Renewable and Sustainable Energy Reviews*. doi: 10.1016/S1364-0321(01)00002-8.

Gabrovšek, R. *et al.* (1993) 'Tobermorite formation in the system CaO, C3SSiO2Al2O3NaOHH2O under hydrothermal conditions', *Cement and Concrete Research*, 23(2), pp. 321–328. doi: 10.1016/0008-8846(93)90097-S.

Ghabezloo, S. *et al.* (2008) 'Poromechanical behaviour of hardened cement paste under isotropic loading', *Cement and Concrete Research*. Elsevier Ltd, 38, pp. 1424–1437. doi: 10.1016/j.cemconres.2012.03.002.

Ghabezloo, S., Sulem, J. and Saint-Marc, J. (2009) 'The effect of undrained heating on a fluid-saturated hardened cement paste', *Cement and Concrete Research*. Elsevier Ltd, 39(1), pp. 54–64. doi: 10.1016/j.cemconres.2008.09.004.

Hong, S. Y. and Glasser, F. P. (2004) 'Phase relations in the CaO-SiO2-H2O system to 200 C at saturated steam pressure', *Cement and Concrete Research*, 34, pp. 1529–1534. doi: 10.1016/j.cemconres.2003.08.009.

IRENA (2017) 'REthinking Energy', *REthinking Energy 2017: Accelerating the global energy transformation*, p. 96.

Kuzielová, E. *et al.* (2017) 'Pore structure development of blended G-oil well cement submitted to hydrothermal curing conditions', *Geothermics*, 68, pp. 86–93. doi: 10.1016/j.geothermics.2017.03.001.

Kyritsis, K. *et al.* (2009) 'Relationship between engineering properties, mineralogy, and microstructure in cement-based hydroceramic materials cured at 200 - 350 C', *Journal of the American Ceramic Society*, 92(3), pp. 694–701. doi: 10.1111/j.1551-2916.2008.02914.x.

Lavrov, A. and Torsæter, M. (2016) *Physics and Mechanics of Primary Well Cementing*. doi: 10.1007/978-3-319-43165-9.

ermal Stresses in Annular Cement', in *Physics and Mechanics of Primary Well Cementing*. doi: 10.1007/978-3-319-43165-9.

Meller, N., Hall, C. and Phipps, J. S. (2005) 'A new phase diagram for the CaO–Al2O3 –SiO2 –H2O hydroceramic system at 200C', *Materials Research Bulletin*, 40, pp. 715–723. doi: 10.1016/j.materresbull.2005.03.001.

Nelson, E.B., Guillot, D. (Eds.), 2006. Well cementing, Second Edi. ed. Schlumberger, Sugar Land, TX 77478, USA.Odelson, J. B., Kerr, E. A. and Vichit-Vadakan, W. (2007) 'Young's modulus of cement paste at elevated temperatures', *Cement and Concrete Research*, 37(2), pp. 258–263. doi: 10.1016/j.cemconres.2006.11.006.

Patchen, F. D. (1960) 'Reaction and Properties of Silica-Portland Cement Mixtures Cured at Elevated Temperatures', *Journal of the Society of Petroleum Engineers*, (219), pp. 281–287.

Pernites, R. B. and Santra, A. K. (2016) 'Portland cement solutions for ultra-high temperature wellbore applications', *Cement and Concrete Composites*. doi: 10.1016/j.cemconcomp.2016.05.018.

Philippacopoulos, A. J. and Berndt, M. L. (2001) 'Mechanical Property Issues for Geothermal Well Cements', *Geothermal Resources Council Transactions*, 25.

Philippacopoulos, A. J. and Berndt, M. L. (2002) 'Structural analysis of geothermal well cements', *Geothermics*, 31. doi: 10.1016/S0375-6505(02)00029-9.

Roy, D. M. (1987) 'New Strong Cement Materials Chemically Bonded Ceramics', *American Association for the Advancement of Science*, 235, pp. 651–658.

Saemindsson, K., Axelsson, G. and Steungrimsson, B. (2009) *Geothermal systems in global perspective*.

Sakai, Y. and Kishi, T. (2017) 'Deformation Mechanism of Hardened Cement Paste and Effect of Water', *Journal of Advanced Concrete Technology*, 15(1), pp. 19–28. doi: 10.3151/jact.15.19.

Shadravan, A. *et al.* (2015a) 'Zonal Isolation in Geothermal Wells', in *PROCEEDINGS, 40th Workshop on Geothermal Reservoir Engineering Stanford University*, p. 10.

Shadravan, A. *et al.* (2015b) 'Zonal Isolation in Geothermal Wells', in *PROCEEDINGS, Fortieth Workshop on Geothermal Reservoir Engineering Stanford University*, p. 10.

Shaw, S., Clark, S. M. and Henderson, C. M. B. (2000) 'Hydrothermal formation of the calcium silicate hydrates, tobermorite (Ca5Si6O16(OH)2 · 4H2O) and xonotlite (Ca6Si6O17(OH)2): An in situ synchrotron study', *Chemical Geology*, 167, pp. 129–140. doi: 10.1016/S0009-2541(99)00205-3.

Taylor, H. F. W. (1990) *Cement chemistry*, *Academic Press Thomas Telford*. doi: 10.1016/S0958-9465(98)00023-7.

Teodoriu, C. *et al.* (2013) 'Wellbore integrity and cement failure at HPHT conditions', *International Journal of Engineering and Applied Sciences*, 2(2), pp. 1–13.

Teodoriu, C. and Falcone, G. (2008) 'Comparison of Well Completions Used in Oil/Gas Production and Geothermal Operations: a New Approach To Technology Transfer', in *PROCEEDINGS, 33rd Workshop on Geothermal Reservoir Engineering*, pp. 1–6.

Terzaghi, K., 1943. Theoretical soil mechanics. J. Wiley, New York.

Thiercelin, M. J. *et al.* (1997) 'Cement Design Based on Cement Mechanical Response', *SPE Annual Technical Conference and Exhibition*, pp. 266–273. doi: 10.2118/38598-MS.

Ulm, F.-J., Constantinides, G. and Heukamp, F. H. (2004) 'Is concrete a poromechanics materials?—A multiscale investigation of poroelastic properties', *Materials and Structures*, 37(1), pp. 43–58. doi: 10.1007/BF02481626.

Vandegrift, D. and Schindler, A. (2006) 'The Effect of Test Cylinder Size on the Compressive Strength of Sulfur Capped Concrete Specimens', (August), pp. 1–83.